national accelerator laboratory

FERMILAB-Conf-74/97-THY/EXP
7100.186

RECENT RESULTS ON NUCLEON DIFFRACTIVE DISSOCIATION*

S. V. Mukhin and V. A. Tsarev†
Joint Institute for Nuclear Research, Dubna, USSR

September 1974

*Invited paper presented at the 1974 Meeting of the Division of Particles and Fields of the American Physical Society, Williamsburg, Virginia.

†Permanent address: Lebedev Physical Institute, Moscow, USSR.

RECENT RESULTS ON NUCLEON DIFFRACTIVE DISSOCIATION

S. V. Mukhin and V. A. Tsarev
Joint Institute for Nuclear Research, Dubna, USSR

I. Introduction

In the past year a lot of interesting data on hadron diffractive dissociation (D. D.) became available. In this paper we shall concentrate on results on D. D. of nucleons in nucleon-nucleon and nucleon-nuclei collisions at high energy and small momentum transfer which give the main bulk of the recent data on D. D. The π- and K-induced D. D. will be mentioned only briefly. We shall discuss D. D. into low and high mass states separately, and we choose to divide them somewhat arbitrarily at $M_x \sim 3$ GeV. In Section II we make a short summary of the properties of low mass D. D. of π- and K-mesons and then in Section III we present in more detail the recent data on low-mass nucleon D. D. Some remarks on the interpretation of these data are given in Section IV. The new data on high mass nucleon excitation are considered in Section V. In Section VI we summarize our conclusions.

II. Diffractive Dissociation of π- and K-Mesons into Low Mass States

Elastic scattering and D. D. have in common the following general properties:

1. Approximately energy-independent cross sections
2. Peripherality

3. Vacuum exchange

4. Approximate factorization

5. Approximately equal cross sections for the dissociation of a particle and its antiparticle.

Apart from these general features D. D. has some interesting specific properties which may probably give us a key to an understanding of this phenomenon.

1. Missing mass distributions in D. D. exhibit strong enhancements in the low mass region (Figs. 1 and 2). Such peaks in mass spectra are usually interpreted as resonances. However, it has been shown recently by detailed spin-parity analysis of D. D. of $\pi \to 3\pi$ in the regions of A_1, A_2, and A_3 peaks[1] and $K \to K\pi^+\pi^-$ near the Q-region[2] that only the $A_2(2^+)$ partial wave has resonance behavior (Figs. 3 and 4). (In fact the situation with the A_3 is not completely clear. The recent measurements in the 11-25 GeV range[3] may indicate that generally the phase of the 2^- states relative to 0^-s, 1^+s, and 1^+p rises across the A_2 mass region (Fig. 5). On the other hand, the data of the CERN-Serpukhov collaboration at 40 GeV/c[1] do not show a comparable rise.)

2. Diffractively produced systems preferentially dissociate into two particles, one of which is always a pion: $X \to X_1 + \pi$:[4] $A_1(1.1) \to \rho\pi$, $A_3(1.65) \to f\pi$, $Q(1.3) \to K^*(0.89)\pi$, $L(1.75) \to K^*(1.42)\pi$, etc. The mass distributions for these enhancements usually peak near the $M_{X_1} + \mu_\pi$ threshold.

3. There is a reciprocal relationship between the slope b of the differential cross section and the mass M_X of the produced system. Typically b ~ 15 $(GeV/c)^{-2}$ near threshold and decreases to 4-5 $(GeV/c)^{-2}$ at large M_X. This is illustrated in Fig. 6 from Ref. 5.

4. In contrast to elastic scattering the diffractive system does not conserve s-channel helicity (for review see Ref. 6).

5. The cross section of the interaction of the produced system with nucleons is found from nuclear reactions to be close to the cross section for the interaction of incoming hadron with nucleons. Thus, recent measurements[7] give $\sigma_{A_1N} = 23 \pm 1.5$ mb for $1.0 < M(3\pi) < 1.2$ GeV and $\sigma_{QN} = 22 \pm 2$ mb for $1.0 < M(K\pi\pi) < 1.4$ GeV.

We shall see later that nucleon D. D. displays esentially the same properties.

III. Low-Mass Nucleon Diffractive Dissociation

1. Bump Structure

a. Missing mass experiments

High energy missing mass experiments have been performed recently at Fermilab with the gas jet target. The DFRR-collaboration measured proton excitation in $pp \to Xp$ at 175, 260, and 400 GeV/c in the range $0.01 < |t| < 0.05$ $(GeV/c)^2$, $1.3 < M_X^2 < 3.7$ GeV^2 [8] and in the reaction $pd \to Xd$ at 50 to 400 GeV/c in the range $0.03 \leq |t| \leq 0.12$ $(GeV/c)^2$, $M_X^2 < 36$ GeV^2. [9,10]

The results with the proton target exhibit two striking features: (i) The cross sections at fixed t are energy independent to within about ±20% uncertainty, and (ii) the data show a sharp peak at $M_X^2 \sim 1.8$ which falls very rapidly as $|t|$ increases (see Fig. 7). The data were analyzed in terms of isobars N(1400), N(1520), and N(1688) but without any background. For N(1400) the mass and width have been found to be approximately 1350 MeV and 165 MeV respectively. The fit of the form $d\sigma/dt = Ae^{bt}$ for N(1400) yielded $A = 6.60 \pm 0.45$ mb $(GeV/c)^{-2}$ and $b = 16.1 \pm 2.7\ (GeV/c)^{-2}$.

In the experiment with deuterium target the same broad enhancement at $M_X \sim 1.4$ GeV was also observed (Fig. 8). For comparison with proton data the effect of deuteron structure was eliminated by dividing out the deuteron "form factor":

$$\left(\frac{d\sigma}{dtdM_X^2}\right)_N = \frac{1}{F_d(t)} \frac{d\sigma}{dtdM_X^2}(pd \to Xd),$$

where

$$F_d(t) = [\sigma_{tot}(pd)/\sigma_{tot}(pp)]^2 e^{bt+ct^2},$$

and $b = 25.9\ (GeV/c)^2$, $c = 60\ (GeV/c)^2$. This corresponds to the assumption that the Glauber corrections for D.D. are the same as for elastic pd scattering at $t = 0$, that the t-dependence introduced by these corrections can be neglected, and the proton and neutron cross sections are equal.

A special slit was used[10] in order to improve the mass resolution. As a result, in addition to a broad enhancement at $M_X \sim 1.4$ GeV, some structure at $M_X \sim 1.7$ GeV has been observed (Fig. 9). The nucleon cross sections extracted from this data were analyzed in terms of N(1400) and N(1700) which gave $M_r \sim 1387 \pm 10$ MeV, $\Gamma = 313 \pm 25$ MeV, $d\sigma/dt$ $(t = 0) = 7.7 \pm 0.5$ mb $(GeV/c)^2$ and $b = 19.0 \pm 2.0$ $(GeV/c)^{-2}$ for the 1.4 GeV enhancement (Fig. 10). The agreement with proton data is reasonable, showing the validity of factorizing the deuteron data in terms of pp data and the deuteron form factor. At the same time the parameters of N(1700) are very unstable to small changes in the parameters of the N(1400) contribution.

The RICC collaboration performed an experiment to search for heavy nucleon resonances.[11] The recoil protons were measured from the reaction $pp \to Xp$ in the region of the Jacobian peak at $|t| = 0.175$ $(GeV/c)^2$ and 0.25 $(GeV/c)^2$. The incident momentum range from 9 to 300 GeV/c was covered continuously by taking data during the acceleration ramp of the Fermilab machine. The result shown in Fig. 11 indicates the presence (at low energies $\sim$ 10 and 20 GeV) of 1700 MeV and 2200 MeV bumps but no significant structure at higher mass.

A comparison of the Fermilab missing mass experiment[10] with previous measurements at low energy[12] is shown in Fig. 12. The extrapolation of these data to $s \to \infty$ is also shown

which has been done[13] by fitting the data at each value of M_X to the form $d\sigma/dtdM_X = a(M_X) + b(M_X)\ s^{-q(M_X)}$. The resulting values of $a(M_X)$ which give the limiting distribution for $s \to \infty$ are seen to be very close to the deuterium data at p = 180 and 270 GeV/c. The low energy data were interpreted in Ref. 12 as the production of the N^* isobar plus a smooth background, shown schematically in Fig. 12 by dashed-dotted lines. The results of the fits at low and high energies is shown in Table I.

Table I

	Slope $(GeV/c)^{-2}$		$d\sigma/dt$ (t = 0) mb GeV^{-2}	
	[12a]	[10]	[12a]	[10]
Δ(1236)	6.4 ± 0.8		8.18 ± 0.05	
N(1400)	24.2 ± 2.5	19.0 ± 2.0	11.6 ± 4.2	7.7 ± 0.5
N(1520)	4.84 ± 0.24		0.91 ± 0.19	
N(1688)	5.12 ± 0.08		2.35 ± 0.36	
N(2190)	3.01 ± 0.17		0.16 ± 0.05	

Thus, if one assumes that the smooth background disappears at high energies, the N(1400) contribution seems to be practically energy independent.

Another assumption about the background was used in Ref. 14 where the entire 1.4 bump was assumed to be a non-resonant threshold enhancement (shown schematically by the solid line in Fig. 12). In this case the contribution of the 1.4 GeV bump decreases with energy and is expected to

approach some limiting value, connected with diffractive contribution.

b. Exclusive data

With exclusive measurements one can separate the missing mass spectrum into different multiplicity channels.

At low energies the nucleon dissociation was recently measured in the following reactions: $pp \to pn\pi^+$, $pp\pi^+\pi^-$, $p\Delta^{++}(1236)\pi^-$ at 12 GeV/c by the BHM collaboration.[15] $pp \to pp\pi^o$, $pn\pi^+$ at 16.2 GeV/c by Gnat et al.[16] In neutron dissociation $n \to p\pi^-$ on nuclei in the range 10 to 28 GeV/c by a Michigan-Princeton group[17] and from 8 to 16 GeV/c by Carithers et al.[18] In pd-collision with single[19] and double[20] pion production at 11.6 GeV/c by Hochman, et al. and at 19 and 28 GeV/c by Hanlon et al.[21]

In all these experiments the one-pion production channel is characterized by a broad enhancement at low mass with a maximum at $M_X \sim 1.3$ GeV, which falls off sharply above 1.7 GeV. A typical mass spectrum is shown in Fig. 13. The apparent absence of any peaks in the mass distribution corresponding to the well known N^* resonances is perhaps the most striking result of these data on one pion production.

On the other hand, the mass distribution in the two pion channel shows marked peaks near $M_X = 1450$ MeV and 1700 MeV[15] (see Fig. 14). The comparison of πN and $\pi\pi N$ channels leads to the following observations:

(a) The low-missing mass enhancement at 1.4 GeV is a combination of two peaks: a 1.3-GeV peak in the πN channel and a 1.45-GeV peak in the $\pi\pi N$ channel. This is illustrated in Fig. 15 from Ref. 21 which shows these experimental distributions at 20 GeV/c. We would like to note, however, that these experimental mass distributions were arbitrary normalized to have equal areas; this seems to overestimate the $\pi\pi N$ contribution.

(b) There is a puzzle with the 1.7 GeV enhancement which is seen in $\pi\pi N$ and not in πN channel. If this enhancement is the N(1688) isobar, then the branching ratio $\pi\pi N$: πN should be 40% : 60%. This led to the suggestion[22] that the 1.7 bump is not a resonance but a $N(1500)\pi$ threshold enhancement.

The lack of "fine structure" in low energy one pion production data becomes particularly puzzling in comparison with the recent ISR measurements of the reaction $pp \to p(n\pi^+)$.[23] Two distinct components of inelastic diffraction scattering were observed at the ISR: narrow peaks and broad bump, which can be interpreted as N^*-isobars and a nonresonant component. The strong forward-backward asymmetry found for this component may be evidence of dominance of the one pion exchange contribution (Deck-type). The comparison of the distributions in the forward and backward hemisphere in the Jackson frame would indicate complicated resonance-background interference structure in the low mass region.

In fact, resonance component has both real and imaginary parts, so one can expect the interference to occur irrespectively of background phase. Nevertheless, it is often neglected in analysis.[12] Preliminary data on neutron dissociation $n \to p\pi^-$ from Fermilab[24] also indicate that the 1.4 GeV enhancement has a structure with peaks at $M_X \sim 1.5$ and 1.7 GeV (Fig. 17). But at the same time, the dramatic forward-backward asymmetry found at ISR was not confirmed at Fermilab (Fig. 18).

2. t-Dependence and the Slope-Mass Correlation

The slope b of the differential cross section $d^2\sigma/dtdM_X^2 = Ae^{bt}$ for proton dissociation from pd inelastic scattering[9] is shown in Fig. 19 as a function of the missing mass M_X. The data clearly show the general trend found for DD: the sharp rise of the $b(M_X)$ near the threshold. The high-mass-resolution data of the same group[10] are shown in Fig. 20. There is a general agreement with Fig. 19, although the slit data are somewhat higher. There is also an indication of decreasing b at values of M_X just near the threshold. It is not clear if it is a real effect or not, but the same tendency for flattening of $b(M_X)$ near threshold seems to be present in the exclusive data on $pn \to pp\pi^-$[21] as seen from Table II.

Table II

$p\pi^-$ Mass Interval (GeV)	Slope Parameter b $(GeV/c)^{-2}$ 19 GeV	28 GeV/c
< 1.25	15.4 ± 1.4	17.1 ± 1.3
1.25 - 1.40	16.2 ± 1.1	17.1 ± 1.3
1.40 - 1.55	8.6 ± 0.6	7.8 ± 0.6
1.55 - 1.80	6.7 ± 0.4	7.6 ± 0.5

Measurements at small t do not show any indication of the forward turnover in inclusive[9] semi-inclusive $pp \to (p\pi^+\pi^-) + X$[25] or exclusive ($pp \to p\pi^- n$[23]) cross sections, which is expected in some theoretical models.

Two interesting features have been observed in the ISR measurement[23] of the $pp \to p\,(n\pi^+)$ cross section (Figs. 21, 22).

(a) Two distinctly different slopes. The first at $|t| < 0.4$ $(GeV/c)^2$ is found to be rapidly decreasing with increasing mass. (Compare Figs. 19, 20). A second smaller slope observed at $|t| < 0.4$ GeV^2 is almost mass independent. At the highest mass the steep slope component disappears. The s-dependence of these slopes is shown in Fig. 23 and are very similar to elastic scattering.

(b) There is indication of a diffractive minimum at $|t| \sim 0.2 - 0.3$ $(GeV/c)^2$ for the excitation of small masses.

3. Isospin Decomposition

Isospin analyses of the reaction $NN \to N\,(N\pi)$ were

reported by Hachman et al.[19] and by Gnat et al.[16] A marked difference in the energy behavior of the $I = \frac{1}{2}$ and 3/2 amplitudes (see Fig. 24) was observed (Fig. 25). The dominance of the $I = \frac{1}{2}$ amplitude at higher energies and its weak energy dependence are characteristic of a diffractive process. The other amplitudes drop sharply with energy.

The CHOW-collaboration[23] also estimated the $I = \frac{1}{2}$ cross section. Extrapolating $d\sigma/dt$ for $pp \to pn\pi^+$ to $t = 0$, they obtained $\sigma(pp \to pn\pi^+) = (270 \pm 80)\mu b$ at $\sqrt{s} = 53$ GeV. Assuming that all observed $(n\pi^+)$ states are produced by diffraction (i.e., $I = \frac{1}{2}$) they have $\sigma(pp \to p(N\pi))_{I = \frac{1}{2}} = 3/2\ \sigma(pp \to pn\pi^+)$ which leads in comparison with low energy data to a dependence on equivalent lab momentum of the form $\sigma = a p_{lab}^{-0.4 \pm 0.1}$ (Fig. 26). This relatively strong energy dependence indicates the importance of a nondiffractive component in this range of kinematical variables. It can be easily accommodated into the double-peripheral mechanism where the s-dependence for $pp \to \pi^+ np$ is translated into the sub-energy s_1 dependence of the πN scattering amplitude having both pomeron and nonpomeron contributions.[26]

4. Helicity

Polar and azimuthal angular distributions of $p\pi^-$ in the n^* c.m. system of the reaction

$$p + n \to n^* + p_{p\pi^-}$$

have been studied by the Vanderbilt group[21] for $|t'| < 0.1$

$(GeV/c)^2$. The results show (Fig. 27): (a) lack of symmetry in the polar angle, particularly for $M(p\pi^-) > 1.4$ GeV which is indicative of an interference between different angular momentum states, (b) the azimuthal distributions are inconsistent with either s- or t-channel helicity conservation. The same conclusion has been recently reached from the coherent excitation of the $\pi^+\pi^-p$ system in the reaction $pd \to pd\pi^+\pi^-$.[27]

5. Absorption in Nuclei

The neutron dissociation into the $p\pi^-$ system on different nuclei from C to U was studied by the Rochester-Brookhaven group.[18] Using the Kolbig-Margolis optical model a cross section of 30-40 mb for scattering of the $(p\pi^-)$ system with $\sim$ 1.4 GeV mass on nucleons was extracted from the data (Fig. 28). The result is in agreement with other measurements and shows that the produced system interacts similarly to the incident hadron.

IV. Some Remarks on Interpretation of the Data

1. The picture of the low missing-mass nucleon spectra which seems to be emerging from the data is the following: there is a strong broad enhancement at $M_X \sim 1.4$ GeV which consists of two bumps $M_X \sim 1.3$ GeV in πN and 1.45 GeV in $\pi\pi N$ channels. On the top and tail of this bump some other narrower peaks are superimposed. Possible candidates are $N^*(1470)$-Roper, $N^*(1520)$, $N^*(1688)$, $N(1700)$-bump and $N^*(2200)$.

2. As was already mentioned, from direct spin-parity analysis it is known that not all bumps in D.D. correspond to resonances. The interesting question is: what is the mechanism causing a "resonance like" enhancement for the nonresonant amplitude at certain mass values? In nucleon D.D. this is a question first of all about the nature of the 1.4 GeV enhancement.

Sometimes there is a tendency to associate the 1.4 GeV bump with the nucleon isobar $N^*(1470)$ (Roper resonance). But this interpretation meets a number of difficulties:

(a) The significant shift of the peak position in production and formation experiments. In $N \to \pi N$ and $N \to \pi\pi N$ channels the peaks are observed at different masses.

(b) The width of the peak is much larger in production than in formation.

(c) The resonance model is not able to explain the strong slope-mass correlation.

Another interpretation of the 1.4 GeV bump (and other diffractive non-resonant enhancements) is connected with Drell-Hiida-Dick-type (DHD) multiperipheral mechanism,[28] corresponding to the diagram shown in Fig. 29a. This model successfully explains many characteristic features of diffractive dissociation: weak s-dependence, approximately equal cross-sections for the dissociation of a particle and

its antiparticle, approximate factorization, predominantly vacuum exchange, preference for dissociation into $X_1 + \pi$ system.

The low-mass enhancement and strong slope-mass correlation in this model are a consequence of kinematics and double preipherality: $T \sim \exp(bt+b_1t_1)$. At the threshold t and t_1 are linearly related and consequently $T \sim \exp[(b+b_1)t]$. At larget M_X the t_1-t connection becomes weaker leading to a weaker t-dependence of T. The difference in peak position for πN and $\pi\pi N$ channels is naturally explained in terms of the different masses of the final states.

The DHD peripheral model in various modifications was successfully applied in analysis of π-K- and N- diffractive dissociation in different regions of kinematical variables. However, recently, some objections have been found against such interpretations of diffraction bumps.

First, in a detailed analysis of the reaction $pp \to pn\pi^+$ as a function of all four variables it was pointed out[29] that pure kinematics is not sufficient to reproduce the whole M_X-dependence of the slope parameter and that the data still show some extra M_X-dependence of the slope which must be explicitly present in the invariant matrix element.

Secondly, the DHD model gives a wrong prediction for the cross-over in $K(\bar{K}) \to Q(\bar{Q})$ diffractive dissociation.[30]

These difficulties are serious problems for the DHD-type model and led to skepticism with its validity.

However, it was shown recently[31] that a way out may be found which is connected with absorption. The idea is to take into account, in addition to the "indirect" interaction via pion emission, the "direct" interaction (wavy lines in Fig. 29b) of the incoming nucleon with the target. Such absorption effects are known to be important in binary reactions. The model displays the following features:

(a) Absorption introduces extra t- (and t_1-) dependence into the amplitude leading to a very steep differential cross section near threshold. This dependence is found necessary from a comparison with experimental data and is usually attributed to off-shell effects. The relative magnitude of the absorptive correction is shown decreasing with M_X due to increasing of the helicity-flip effects leading to a decrease of the slope of the amplitude at larger M_X.

(b) At some $t = t^*$ a diffractive minimum is predicted which disappears at larger M_X. A rough estimate gives $|t^*| \sim 0.2$ $(GeV/c)^2$ in agreement with the data (Fig. 22).

(c) It may be possible to explain the cross-over in $K(\bar{K}) \to Q(\bar{Q})$ but at present it is difficult to say anything more definitive since the K^*N scattering amplitude entering into the absorptive corrections is unknown.

The measurement of the cross-over for reactions such as

$$pp \to \pi^+ np \ (\pi^o pp), \quad pp \to \pi^- n^- p \ (\pi^o n^- p)$$

can be a crucial test because the absorptive corrections

can be expressed in terms of known values of cross sections and slopes for pp and $p\bar{p}$ scattering.

If the final-state scattering is known the model will involve no free parameters, in comparison with the usual DHD model, and it gives predictions for dependence on all variables.

The detailed comparison of the model with experiment has not been done yet.

3. Another experimental fact which is usually considered as evidence against DHD-type models is a small cross section for interaction of the diffractively produced system in nuclei. The popular approach for explanation of this phenomenon is based on Pomeranchuk's idea[32] that at the early stages of production processes the hadronic matter is confined in a region of size $\lesssim$ 1 fermi and does not have a definite number of particles due to strong creation and absorption of virtual particles. Then the cross section for the interaction of this system can be much smaller than the sum of cross sections for all final particles, as observed in experiments.

However, the multiperipheral model suggests another picture of particle production. Particles are created over an extended region of space-time.[33] In particular, some of the particles are created before the projectile reaches the target and they miss the target. This leads to a decrease

of the nuclear scattering of produced particles, the usual cascades do not develop in the nucleus and the DHD-type multiperipheral models can also be reconciled with experiment.

4. The slope-mass correlation for nucleon D.D. has been also discussed by Humble[34] on the basis of a general approach suggested by Kane.[30] Peripheral impact profiles for each helicity amplitude were assumed, so that helicity amplitudes have the form

$$T_{\Delta\lambda}^{J}(s,t_1 M_X^2) \sim e^{at} J_{\Delta\lambda}(R\sqrt{-t})$$

($J_{\Delta\lambda}(x)$ is the Bessel function) and $d\sigma/dtdM_X^2 \sim \sum_{J,\Delta\lambda} |T_{\Delta\lambda}|^2$. At small masses the main contribution is assumed to come from the nonflip amplitude. Then $d\sigma/dt \sim J_o^2(R\sqrt{-t})$ is a steep function of t. For $R \sim 1$ fermi the first zero is expected at $|t| \sim 0.2$ $(GeV/c)^2$. At larger M_X the differential cross section becomes more flat due to helicity-flip contributions. To describe the impact profile, relative strength of different helicity amplitudes and the shape of mass distributions, the model introduces a number of phenomenological parameters.

5. One of the possible reasons for the absence of resonance structure in the neutron dissociation experiment[17] may be connected with a specific feature of the experimental set up: insensitivity to decays with $\theta_\pi^* \gtrsim 90^o$. The efficiency was calculated assuming a symmetrical distribution

of about 90°. The ISR data[23] indicates that the forward-backward asymmetry may be significant. The other possibility is a dip in the $N^{*}(1688)$ production for $-t < 0.05$ $(GeV/c)^2$. The forward dips (due to the vanishing of helicity-flip amplitudes), as a reason for the absence of N^{*} in neutron dissociation, have been discussed in Ref. 35. The problem of experimentally recognizing such forward dips in cross sections for N^{*} production is complicated due to uncertaintly with background.

Apart from the trivial kinematical (spin) reason for this forward turnover, there may be some other, more fundamental reason to expect it in diffractive dissociation amplitudes. If the total hadronic cross sections approach constant limits at infinite energies, then one of the consequences will be a vanishing of diffractive dissociation cross sections at $t \simeq -q_{\perp}^2 = 0$ <u>for any mass of the produced system</u>.[36] Existing experimental data do not show the forward turnover either in the low or large mass region. However, the accessible energies may be far from asymptotical.

V. Diffractive Proton Dissociation into High Mass States

Recent data on proton D.D. into high mass states have already been excellently reviewed at the APS meeting in 1973 by Leith.[37] So, in this section we shall discuss only new results, obtained after that meeting.

1. The DFRR collaboration[9] has studied the coherent

low momentum transfer interaction of high energy protons with a deuterium gas jet target $p + d \to X + d$ in the range $50 < p < 400$ (GeV/c), $0.03 < |t| < 0.12$ $(GeV/c)^2$ and $M_X^2 < 35$ GeV^2. The results are presented in Figs. 30-33 in terms of the cross section "per nucleon". These figures show the following essential features:

(a) The cross sections are consistent with energy independence to within $\sim$ 10% over the entire missing mass range within $X > \sim 0.97$. However, the 50 GeV/c data seem to be consistently higher.

(b) For $M_X^2 \gtrsim 6$ GeV^2 the points in Fig. 30 lie on a horizontal line within errors, indicating a $1/M_X^2$ behavior for the cross section. The same behavior is observed for other t values in this mass region.

(c) The slope parameter appears to be energy independent. It decreases rapidly as a function of M_X^2 from a value of ~ 18 $(GeV/c)^{-2}$ at $M_X \sim 1.8$ GeV^2 to become constant, within errors, at ~ 5.5 $(GeV/c)^{-2}$ for $M_X^2 > 6$ GeV^2.

(d) The integral of M_X^2 $d\sigma/dt dM_X^2$ over t seems to be a constant in s and M_X^2 for all mass values in the interval considered, $x \gtrsim 0.97$: $d\sigma/dM_X^2 \simeq 0.7$ M_X^{-2} mb GeV^{-2}. The plot of the cross section in terms of the Feynman scaling variable X is shown in Fig. 33. All points (except those below M_p^2/s) lie approximately on the same straight line. These data were analyzed in terms of a simple model.[14]

The low mass peak was described by a DHD type amplitude. At large M_X it was suggested that only the PPP term was important. The value of $G_{PPP}(t)$ has been calculated from the low mass contribution using the finite mass sum rule.[38] The important point about this calculation is that both elastic and Deck terms contribute to $G_{PPP}(t)$. If confirmed by more detailed data and analysis this will support the idea[39] that unlike hadronic cross sections, resonances and background contribute to the Pomeron in Pomeron-hadron scattering. The result of the calculations is shown in Figs. 30, 31 and the corresponding Pomeron-proton cross section in Fig. 34.

We want to stress here that the approximate constancy of $M_X^2\, d\sigma/dtdM_X^2$ which motivated the simple model with only the PPP term, can be also the result of a chance interplay of different triple Regge terms. This is illustrated by curve 2 of Fig. 35 which has been calculated with P and R contributions found in Ref. 40. Using $\alpha_R(0) = 0.4$ instead of 0.5 used in Ref. 40 (but with the same values of $G_{ijk}(t)$) leads to curve 3.[41]

The other remark with respect to comparison of deuteron and nucleon data is that the isospin selection eliminates ρ, A_2 and π- contributions for the deuteron case. The π- contribution is particularly important for nucleon at small $X = 1 - M_X^2/s$. The effect of $\pi\pi R$ and $\pi\pi P$ terms can be seen from comparison of the curves 1 (with $\pi\pi R$ and $\pi\pi P$) and 2

(without these terms).

2. This pion contribution can be directly obtained from measurements of the pd → pX cross section performed on a deuteron jet target by RICI group.[42] Combining this data (Fig. 36) with their previous results on pp → Xp the authors extracted the invariant cross section for charge exchange inelastic scattering p + n → p + X shown in Figs. 37, 38. The following assumptions were used. pd → pX cross sections were multiplied by 1.05 to correct for the shadowing effect. From the resulting cross sections they subtracted the pp-elastic and pp → pX inclusive cross sections both of which were Fermi smeared, corrected for coherent pd scattering (by including the deuteron form factor) and corrected for rescattering off the spectator neutron. The prediction of the triple Regge model with $\pi\pi R$ and $\pi\pi P$ terms from Ref. 40 as seen in Fig. 38 is in good agreement with the data.

VI. Conclusions

1. The low mass nucleon excitation spectrum is a superposition of a broad nonresonant enhancement at $M_X \sim$ 1.4 GeV (which consists mainly of a 1.3 GeV bump in the πN channel and a 1.45 GeV bump in the $\pi\pi N$ channel) and narrow peaks at $M_X \sim$ 1.47 (?), 1.5, 1.7, and 2.2 GeV. Experimental data are still contradictory on some important features of the structure of D.D. cross section. Further work is needed to clarify the situation with respect to "fine" structure of

the bump and forward-backward asymmetry.

2. A good candidate for the mechanism for nonresonant enhancements in D.D. mass distribution is Drell-Hiida-Deck model modified by absorption.

3. The forward peak in the low mass D. D. cross section shrinks similarly to the elastic pp cross section.

4. The dip in $d\sigma/dt$ for small M_X indicates the peripherality of the low-mass production amplitude.

5. There is no experimental evidence for the forward turnover in the D.D. cross section.

6. s-channel helicity nonconservation may play an important role in D.D., in particular in the slope-mass correlation and dip structure.

7. The triple Pomeron coupling may be quite large ($G_{PPP}(0) \sim 4$ mb GeV^{-2}). There is no indication of its turnover at small t. The compilation of values of $G_{PPP}(t)$ at small t from recent analyses are presented in Fig. 39. An abnormal type duality for the Pomeron-particle amplitude has some support from the analysis of recent high M_X-data.

In conclusion we would like to say that the new data give us better understanding of some important features of diffractive dissociation. Nevertheless, the whole picture is still obscure. Is the animal which we touch in diffractive dissociation the elephant, mentioned by Dr. Dao in his talk or does it look more like that in Fig. 40? We hope

we shall sometime be able to answer this question.

Acknowledgements

We are very grateful to G. C. Fox, E. Malamud, and W. Baker for useful discussions.

References

1. G. Ascoli et al., Phys. Rev. Letters 25, 962 (1970); Phys. Rev. Letters 26, 929 (1971); Phys. Rev. D7, 669 (1973); CERN-Serpukhov Collaboration Y. M. Antipov et al., Nucl. Phys. B63, 153 (1973).
2. Aachen-Berlin-CERN-London-Vienna Collaboration, M. Deutschmann et al., Phys. Letters B49, 388 (1974).
3. Aachen-Berlin-Bonn-CERN-Heidelberg Collaboration, G. Otter et al., CERN/D.Ph. II/PHYS 74-21 (1974) to be published in Nucl. Phys. B; G. Thompson et al., Phys. Rev. Letters 32, 331 (1974).
4. H. J. Lubatti, Acta Phys. Polon. B3, 721 (1972).
5. H. J. Lubatti, K. Moriyasu preprint VTL-PUB-18 (1974).
6. G. Otter, Acta Phys. Polon. B3, 809 (1972).
7. C. Bemporad et al., papers 215 and 216 presented to the Aix-en-Provence conference 1973.
8. Duban-Fermilab-Rockefeller-Rochester Collaboration, B. Bartenev et al., Phys. Letters B51, 299 (1974).
9. Y. Akimov et al., NAL-Conf-74/56 Exp (1974).
10. Y. Akimov et al., NAL-Conf-74/66 Exp (1974).
11. K. Abe et al., paper submitted to this meeting.
12. E. W. Anderson et al., Phys. Rev. Letters 16, 854 (1966). R. M. Edelstein et al., Phys. Rev. D5, 1073 (1972);
(a) J. V. Allaby et al., Nucl. Phys. B52, 316 (1973).
13. P. H. Frampton and P. V. Ruuskanen, Phys. Letters 38B, 78 (1972).

14. Y. Akimov et al., Fermilab-Conf-74/79-THY/Exp (1974).

15. Bonn-Hamburg-Munchen Collaboration, P. Kobe et al., Nucl. Phys. B52, 109 (1973).

16. Y. Gnat et al., Nucl. Phys. B54, 333 (1973).

17. D. D. O'Brien et al., Nucl. Phys. B77, 1 (1974).

18. W. C. Carithers et al., paper submitted to this meeting.

19. D. Hochman et al., WIS-FY/18 Ph (1974).

20. H. Hochman et al., WIS-74/13 Ph (1974).

21. J. Hanlon et al., paper submitted to this meeting.

22. H. J. Lubatti, Proceedings of the Internation Conference on Elementary Particles, Aix-en-Provence p. 277.

23. CERN-Hamburg-Orsay-Vienna Collaboration, E. Nagy et al., Paper submitted to the XVII International Conference on High Energy Physics, London, 1974.

24. Northwestern-Rochester-Massachusetts-Fermilab Collaboration. We would like to thank R. Ruchti for providing us with information on this data.

25. Aachen-Los Angeles-CERN Collaboration, L. Baksay et al., Paper submitted to London Conference, 1974.

26. G. C. Fox, Proc. of Intern. Conf. on High Energy Collisions, Stony Brook, 1973; V. A. Tsarev, to be published.

27. J. W. Chapman et al., Phys. Rev. Letters 30, 64 (1973).

28. S. D. Drell and K. Hiida, Phys. Rev. Letters 7, 199 (1961); R. Deck, Phys. Rev. Letters 13, 1969 (1964).

29. H. I. Mittinen and P. Pirila, Phys. Letters 40B, 127 (1972).

30. G. L. Kane, Acta Phys. Polon. B3, 845 (1972).

31. V. A. Tsarev, Fermilab Pub 74/80 (1974).

32. I. Pomeranchuk, Dokl. Akad. Nauk USSR, 78, 889 (1951).

33. V. N. Gribov, Yad. Fiz. 9, 640 (1969); (Sov. J. Nucl. Phys. 9, 369 (1969)).

34. S. Humble, Ref. TH.1827 CERN (1974).

35. G. Cohen-Tannoudji, G. L. Kane and C. Quigg, Nucl. Phys. B37, 77 (19

36. V. N. Gribov, Proceedings of the Batavia Conference 1972.

37. D. W. G. S. Leith, Invited paper at 1973 APS Meeting, Berkeley.

38. M. B. Einhorn, J. Ellis, and J. Finkelstein, Phys. Rev. D5, 2063 (1972).

39. M. B. Einhorn, M. B. Green, and M. A. Virasoro, Phys. Rev. D7, 102 (1973).

40. R. D. Field and G. C. Fox, CALT-08-434.

41. We appreciate G. Fox providing us with these curves.

42. B. Robinson et al., paper submitted to this meeting.

43. D. R. O. Morrison, Rapporteur's talk, Kiev Conference on High Energy Physics, 1970.

44. D. P. Roy and R. G. Roberts, RL-74-022,T79 (1974).

45. D. Amati, L. Caneschi, M. Ciafaloni, Nucl. Phys. B62, 173 (1973).

46. Y. M. Kazarinov et al., to be published.

47. M. G. Albrow et al., Nucl. Phys. B54, 6 (1973).

48. A. Capella, Phys. Rev. D8, 2047 (1973).

49. A. B. Kaidalov et al., Phys. Letters 45B (1973).

Figure Captions

1, 2. Bump structure in the mass spectrum for 3π and $\pi\pi K$ systems (Ref. 43).

3, 4. Partial waves for 3π[1] and $\pi\pi K$[2] systems near peak positions. Only $2^+(A_2)$ has resonance behavior.

5. Complex behavior of phases 2^-s and 2^-p relative to 0^-s, 1^+s, and 1^+p near the A_3 position found in Ref. 3.

6. A compilation of data on the slope-mass correlation from Ref. 5 shows a sharp rise of b near threshold.

7- 9. Broad bump in the missing mass spectrum in reactions (7) $pp \to Xp$,[8] (8) and (9) $pd \to Xd$.[9,10]

10. Compilation of data on the t-dependence of the $N^*(1400)$ "isobar" production cross section.[10]

11. Missing mass spectrum in $pp \to Xp$ shows peaks at $M_X \sim 1.7$ and 2.2 GeV but no structure at higher masses.[11]

12. Comparison of high[10] and low[12] energy data on missing mass in $pp \to Xp$. Low energy data extrapolated to $s \to \infty$ are in good agreement with high energy data. Solid and dashed-dotted curves correspond to Deck-type and polynomial background.

13. Data on $N \to \pi N$ dissociation at low energies do not show "fine" resonance structure.

14. The mass spectrum for the $\pi\pi N$ system[15] shows peaks at 1.45 and 1.7 GeV.

15. Superposition of 1.3 GeV and 1.45 GeV peaks in the πN and $\pi\pi N$ channels gives a broad bump at 1.4 GeV.[21]

16. The mass spectrum for the $n\pi^+$ system[23] has strong forward-backward asymmetry in the Jackson frame. For $\cos\theta_j < o$ narrow peaks on the top of broad enhancements are seen.

17. The mass spectrum for $p\pi^-$ system obtained from neutron dissociation.[24]

18. Azimutal distribution for the $p\pi^-$ system from neutron dissociation[24] does not show the dramatic asymmetry found at ISR.[23]

19, 20. Slope-mass correlation in $pd \to Xd$.[9,10]

21, 22. Differential cross section for the reaction $pp \to n\pi^+p$ at ISR energies[23] displays two slopes at $|t| \lesssim 0.4$ $(GeV/c)^2$. At small masses of the $(n\pi^+)$ system data indicate diffractive minimum at $|t| \sim 0.3$ $(GeV/c)^2$ which dissapears at large M_X.

23. Shrinking of the $pp \to n\pi^+p$ cross section[23] is similar to elastic scattering.

24. Isospin amplitudes for the reaction $NN \to NN\pi$.

25. Energy dependence of different isospin contributions.[19] The $M^{O}_{\frac{1}{2}}$ (diffractive) component has weak s-dependence and dominates at higher energies.

26. Energy dependence for $(pp \to NN\pi)_{I=\frac{1}{2}}$ cross section from Ref. 23.

27. Polar and azimutal distribution for $p\pi^-$ system[21] are inconsistent with either s- or t-channel helicity conservation.

28. Absorption of $p\pi^-$ system on different nuclei.[18]

29. (a) Drell-Hiida-Deck-type diagram; (b) the same with absorption.

30- 33. Data on nucleon excitation in the reaction $pd \to Xd$.[9] Solid curves correspond to the model of Ref. 14.

34. Pomeron-proton total cross-section found in Ref. 14 from $pd \to Xd$ data.

35. Comparison of the data from Ref. 9 with solution 1 of Ref. 40 including all triple Regge terms possible in reaction $pp \to Xp$ - curve 1. Curve 2 - solution 1 with $\pi\pi R$ and $\pi\pi P$ terms removed (they do not contribute to reaction $pd \to Xd$). Curve 3 - the same as 2 but with $\alpha_R(0) = 0.4$. All curves are lowered by 17%.

36. Cross section for the reaction $pd \to pX$.[42]

37. Different contributions used in extraction of the $pn \to pX$ cross section from $pd \to pX$ data.[42]

38. Cross sections for the reaction $pn \to pX$.[42] Curves correspond to the contribution of the sum of $\pi\pi R$ and $\pi\pi P$ terms from Ref. 40.

39. Compilation of $G_{ppp}(t)$ at small t from some recent analysis. 1 - Ref. 44, 2 - Ref. 14, 3 - Ref. 45, 4 - solution 1 of Ref. 46, 5 - Ref. 47, 6 - solution 1 of Ref. 40, 7 - Ref. 48, 8 - Ref. 49.

40. What we really see in diffractive dissociation(?)

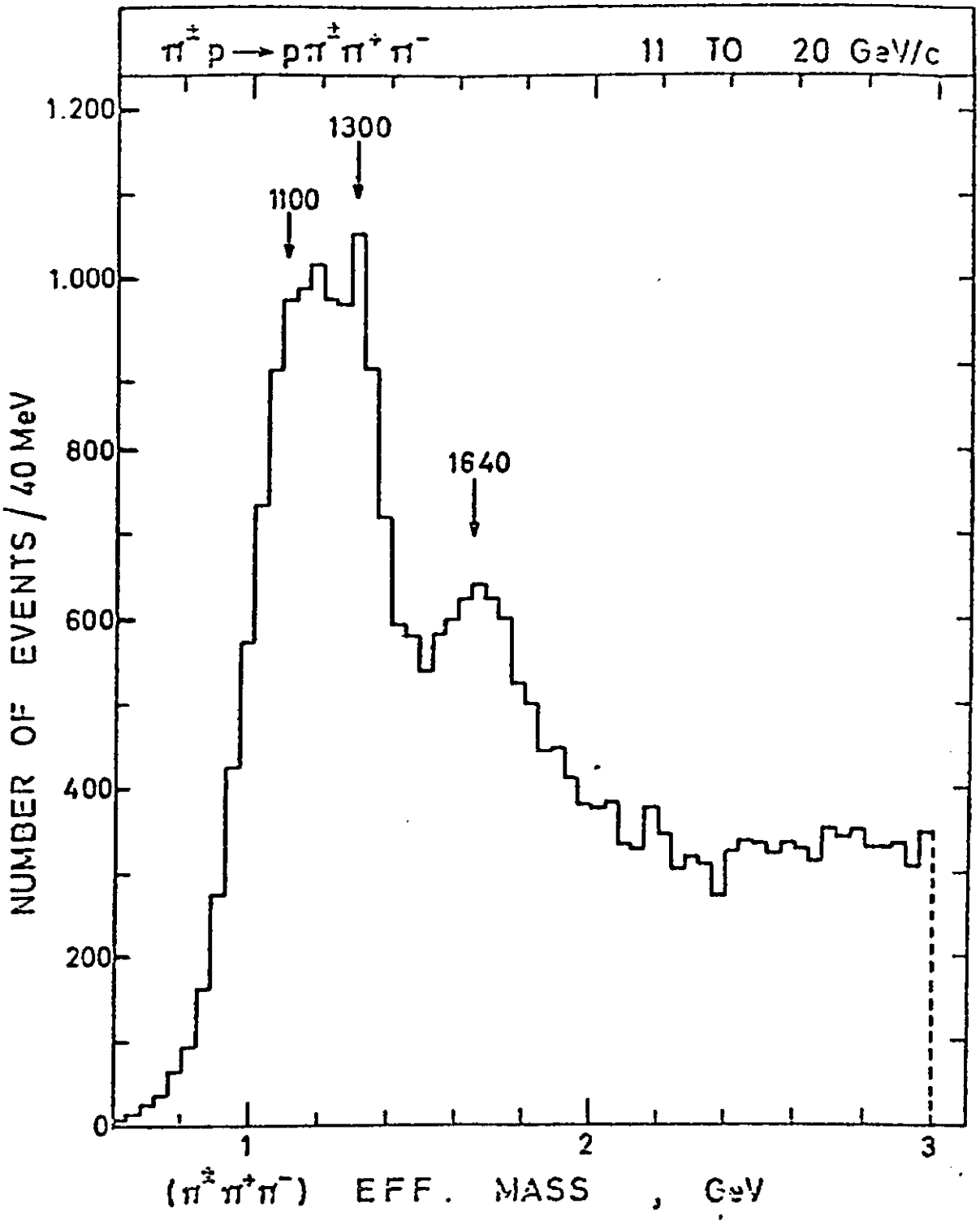
$\pi^{\pm} p \rightarrow p\pi^{\pm}\pi^{+}\pi^{-}$
11 TO 20 GeV/c
1300
1100
1640
1.200
1.000
800
600
400
200
0
1
2
3
NUMBER OF EVENTS / 40 MeV
$(\pi^{\pm}\pi^{+}\pi^{-})$ EFF. MASS , GeV

FIG. 1

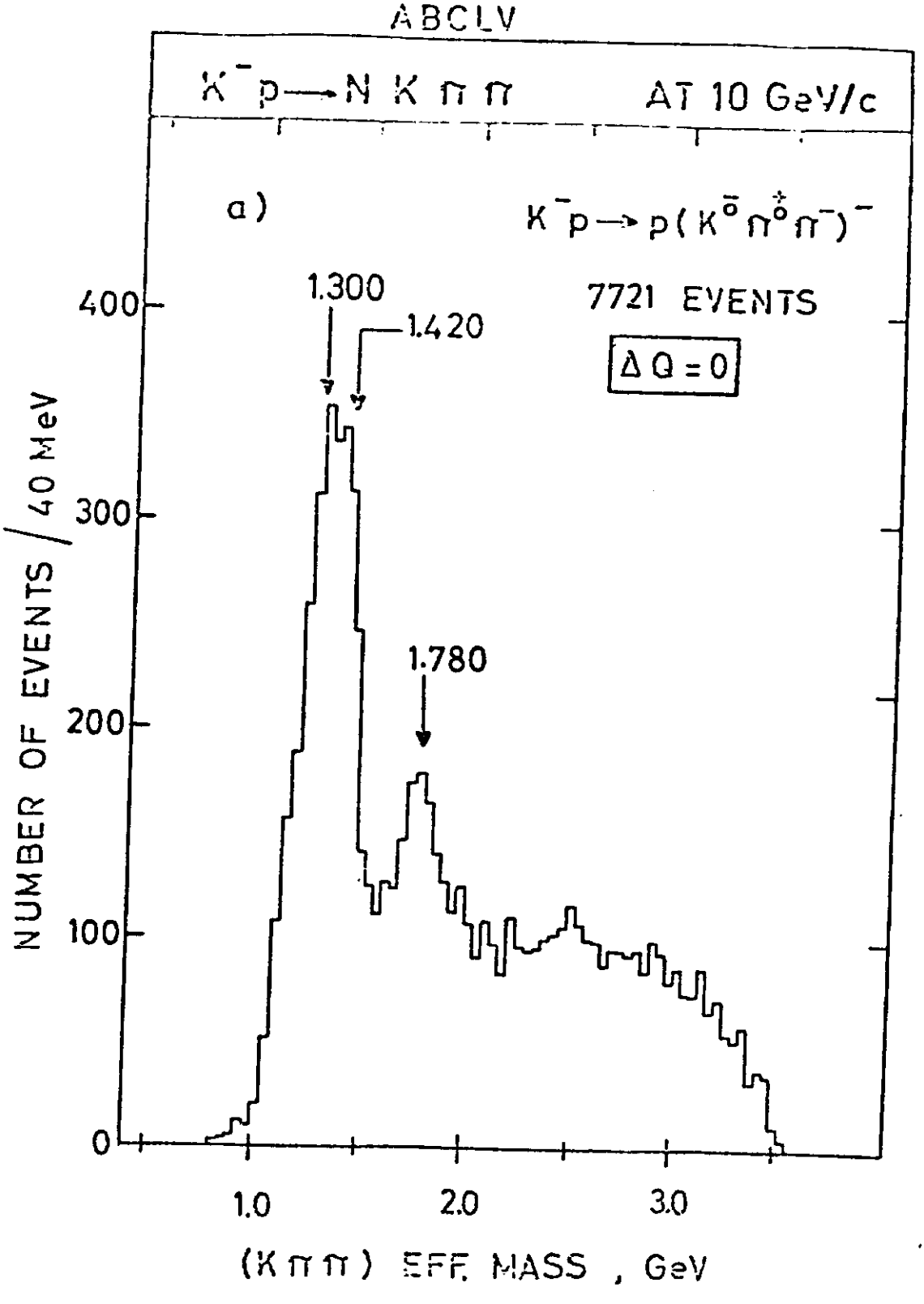
ABCLV
K⁻p → N K π π AT 10 GeV/c
a)
K⁻p → p(K⁰ π⁰ π⁻)⁻
7721 EVENTS
ΔQ = 0
1.300
1.420
1.780
NUMBER OF EVENTS / 40 MeV
400
300
200
100
0
1.0
2.0
3.0
(K π π) EFF. MASS , GeV

FIG. 2

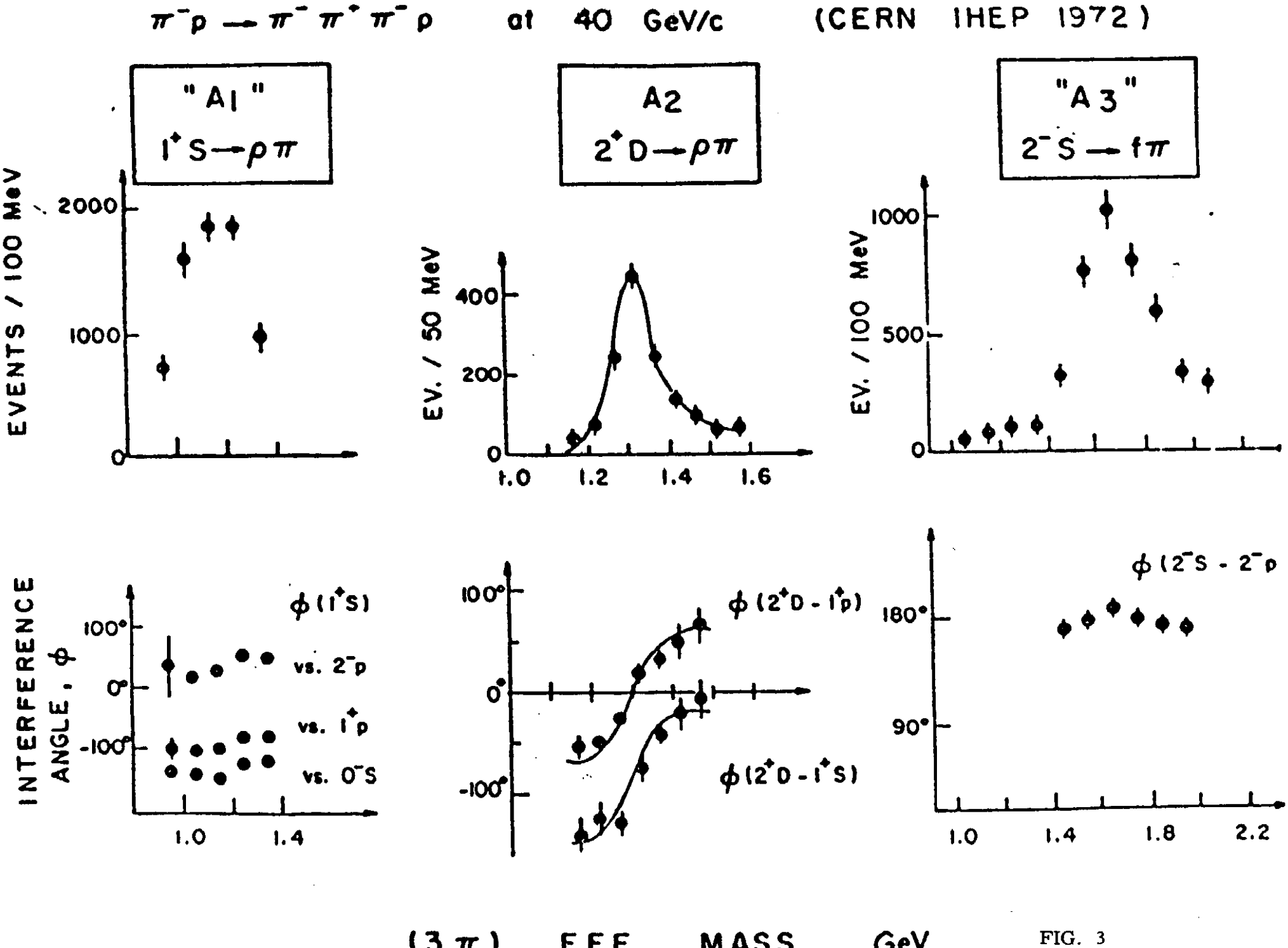
$\pi^- p \to \pi^- \pi^+ \pi^- p$ at 40 GeV/c (CERN IHEP 1972)
"A1"
$1^+S \to \rho\pi$
A2
$2^+D \to \rho\pi$
"A3"
$2^-S \to f\pi$
EVENTS / 100 MeV
EV. / 50 MeV
EV. / 100 MeV
INTERFERENCE ANGLE, ϕ
$\phi(1^+S)$ vs. 2^-p
$\phi(1^+S)$ vs. 0^-S
$\phi(2^+D - 1^+p)$
$\phi(2^+D - 1^+S)$
$\phi(2^-S - 2^-p)$
(3π) EFF. MASS, GeV

FIG. 3

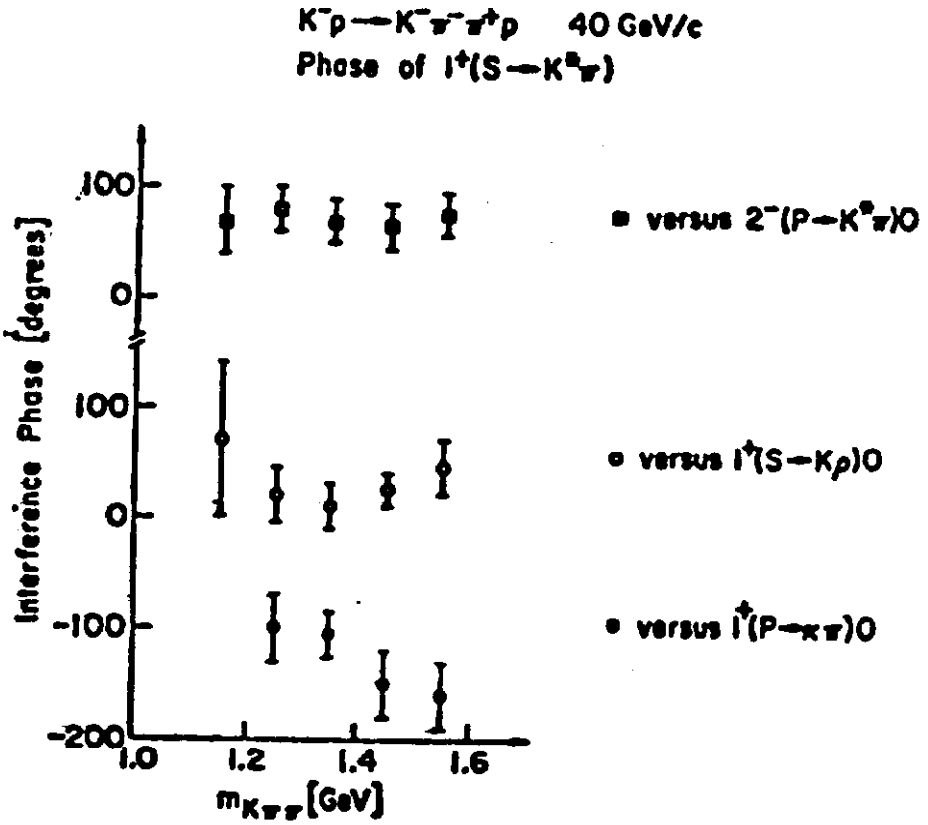
$K^-p \to K^-\pi^-\pi^+p$ 40 GeV/c
Phase of $1^+(S-K^*\pi)$
Interference Phase [degrees]
100
0
100
0
-100
-200
1.0
1.2
1.4
1.6
$m_{K\pi\pi}$ [GeV]
versus $2^-(P-K^*\pi)0$
versus $1^+(S-K\rho)0$
versus $1^+(P-\kappa\pi)0$

FIG. 4

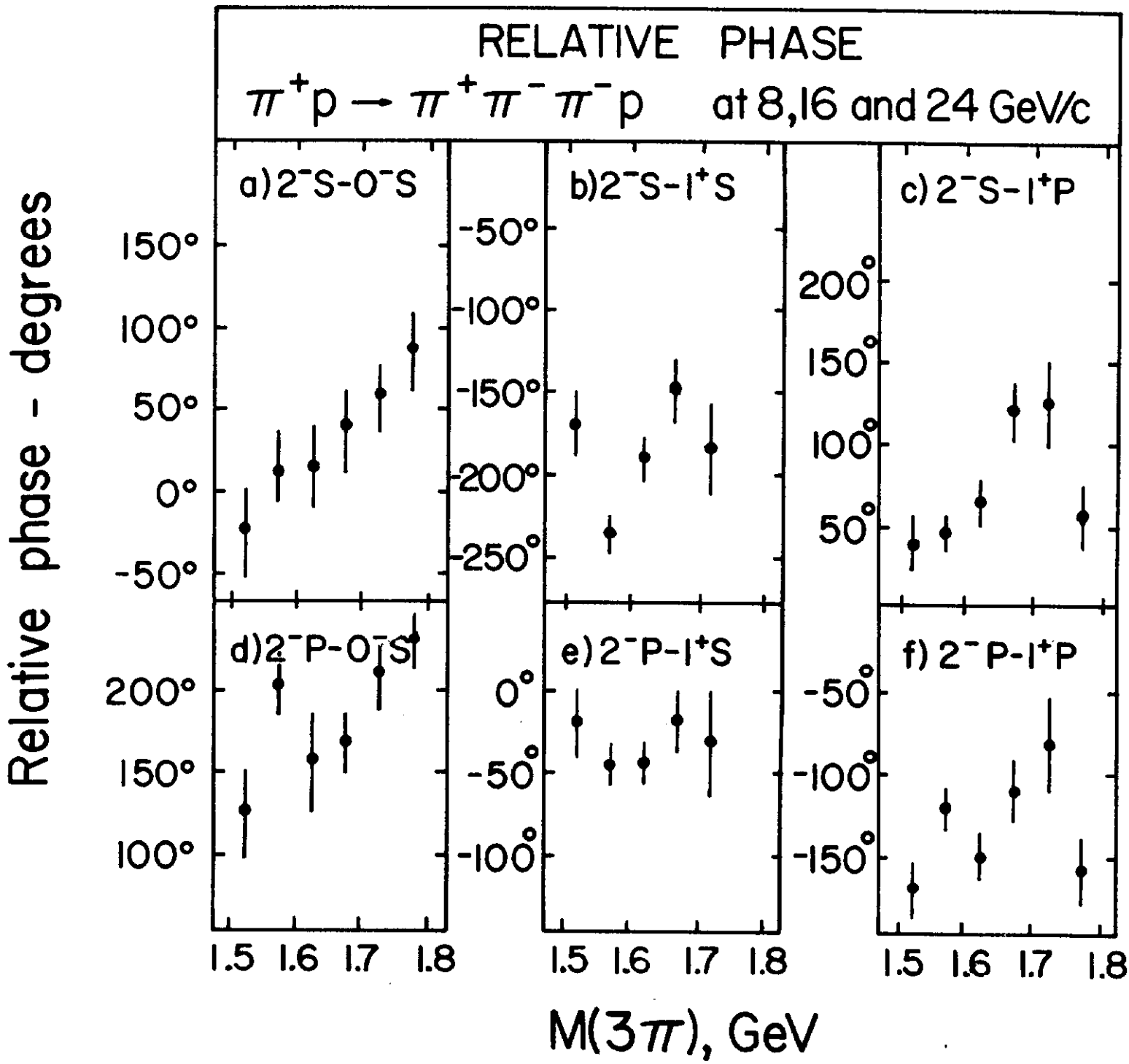
RELATIVE PHASE
$\pi^+ p \to \pi^+ \pi^- \pi^- p$ at 8,16 and 24 GeV/c
a) 2^-S-0^-S
b) 2^-S-1^+S
c) 2^-S-1^+P
d) 2^-P-0^-S
e) 2^-P-1^+S
f) 2^-P-1^+P
Relative phase - degrees
150°
100°
50°
0°
-50°
-50°
-100°
-150°
-200°
-250°
200°
150°
100°
50°
200°
150°
100°
0°
-50°
-100°
-50°
-100°
-150°
1.5 1.6 1.7 1.8
1.5 1.6 1.7 1.8
1.5 1.6 1.7 1.8
M(3π), GeV

FIG. 5

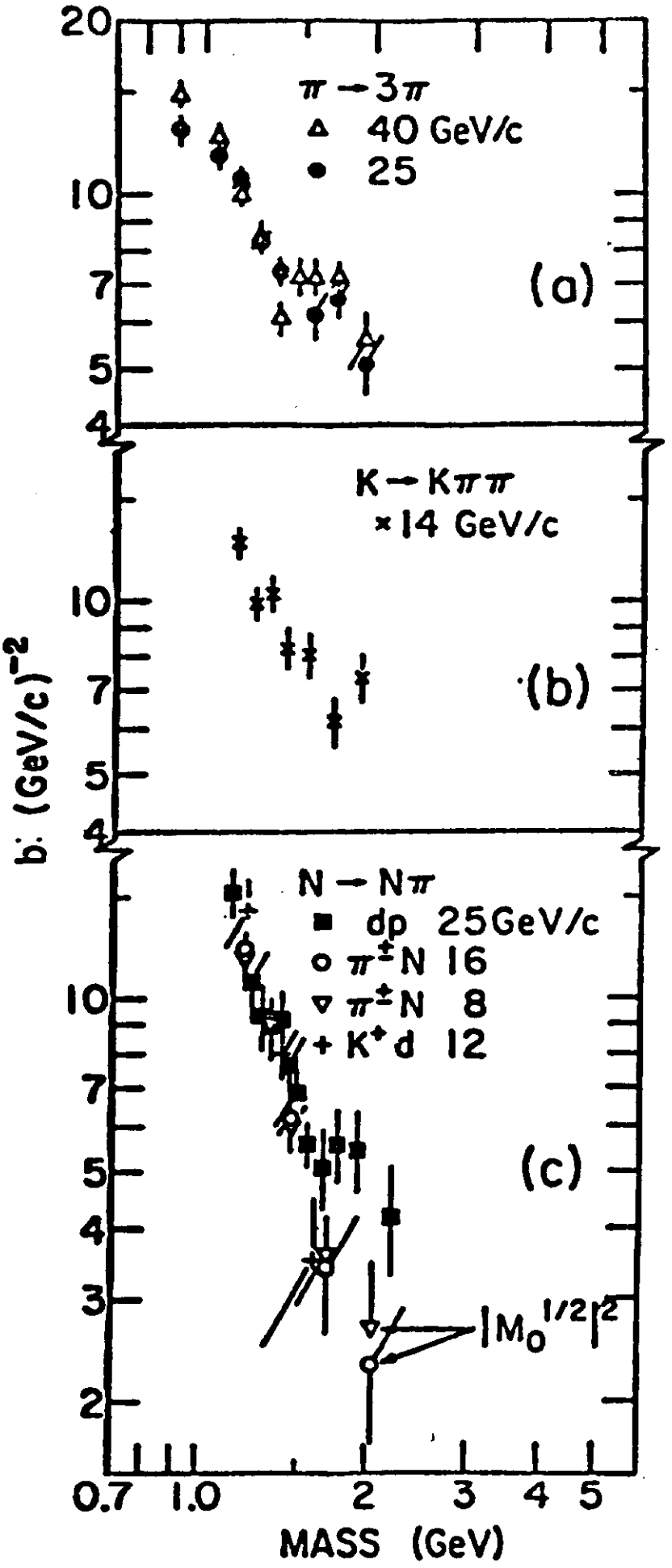
20
10
7
5
4
π − 3π
40 GeV/c
25
(a)
K − Kππ
×14 GeV/c
(b)
N − Nπ
dp 25GeV/c
π±N 16
π±N 8
+ K⁺d 12
(c)
|M₀^1/2|²
b: (GeV/c)⁻²
0.7
1.0
2
3
4
5
MASS (GeV)

FIG. 6

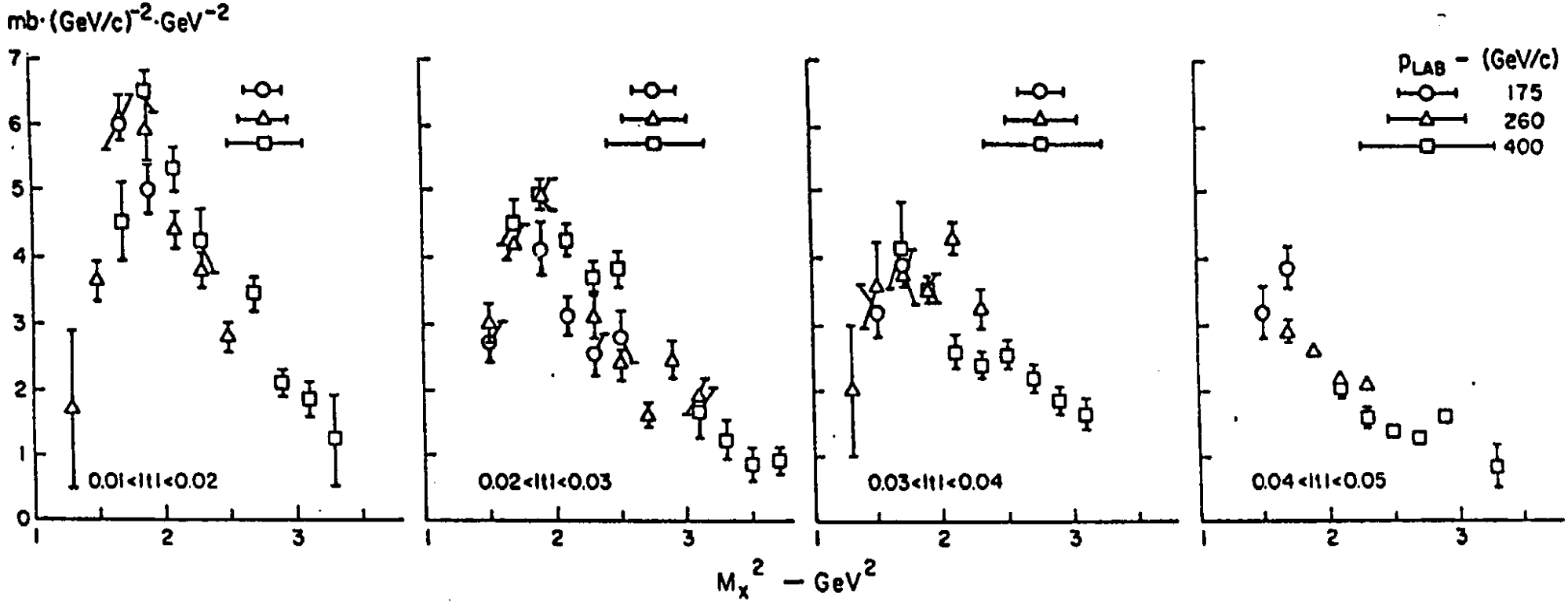
mb·(GeV/c)$^{-2}$·GeV^{-2}
p_{LAB} - (GeV/c)
175
260
400
0.01<|t|<0.02
0.02<|t|<0.03
0.03<|t|<0.04
0.04<|t|<0.05
M_x^2 — GeV^2

FIG. 7

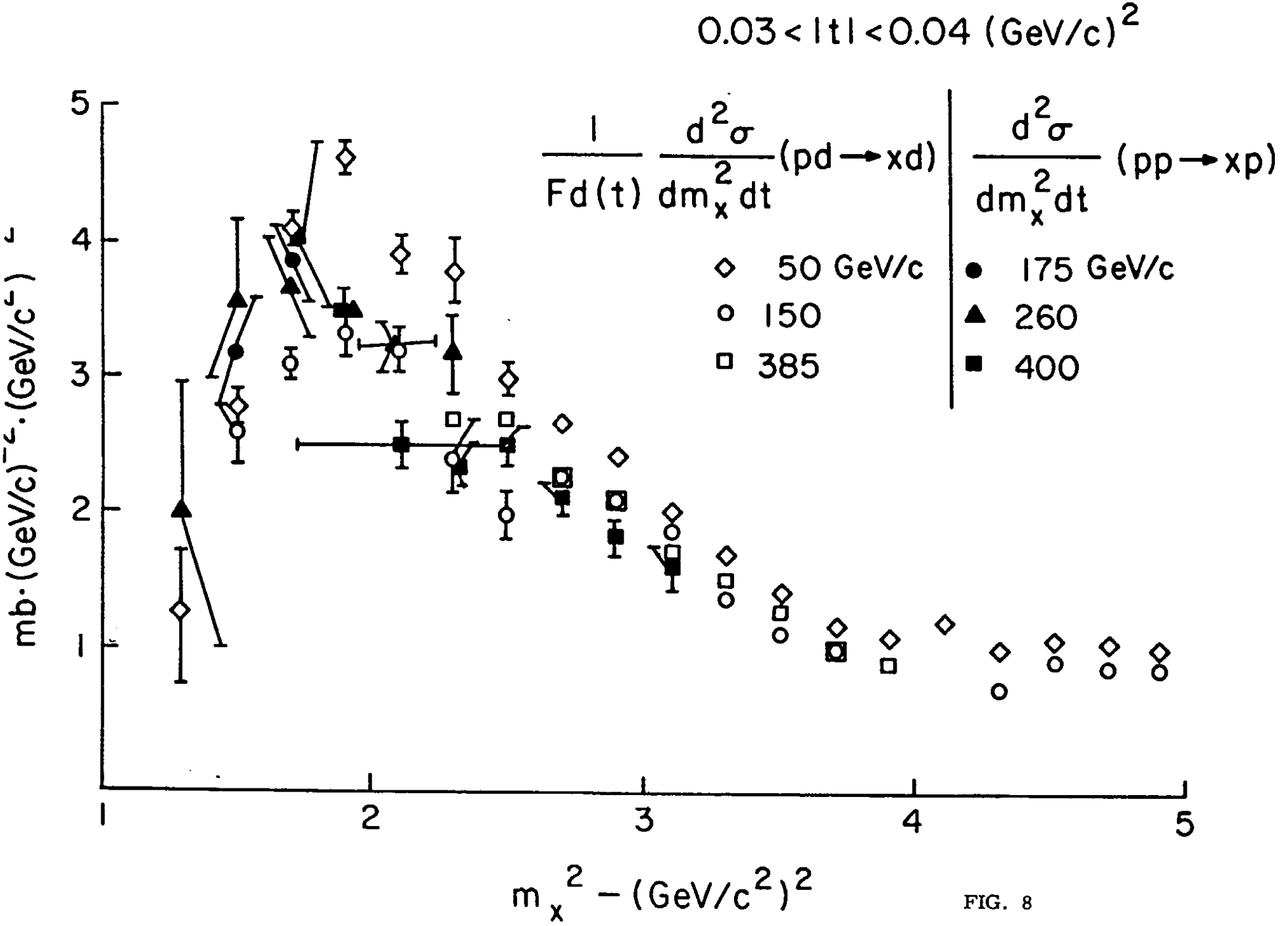
0.03 < |t| < 0.04 (GeV/c)²
1/Fd(t) d²σ/dm_x²dt (pd → xd) | d²σ/dm_x²dt (pp → xp)
50 GeV/c
150
385
175 GeV/c
260
400
mb·(GeV/c)⁻²·(GeV/c²)
m_x² − (GeV/c²)²
1
2
3
4
5

FIG. 8

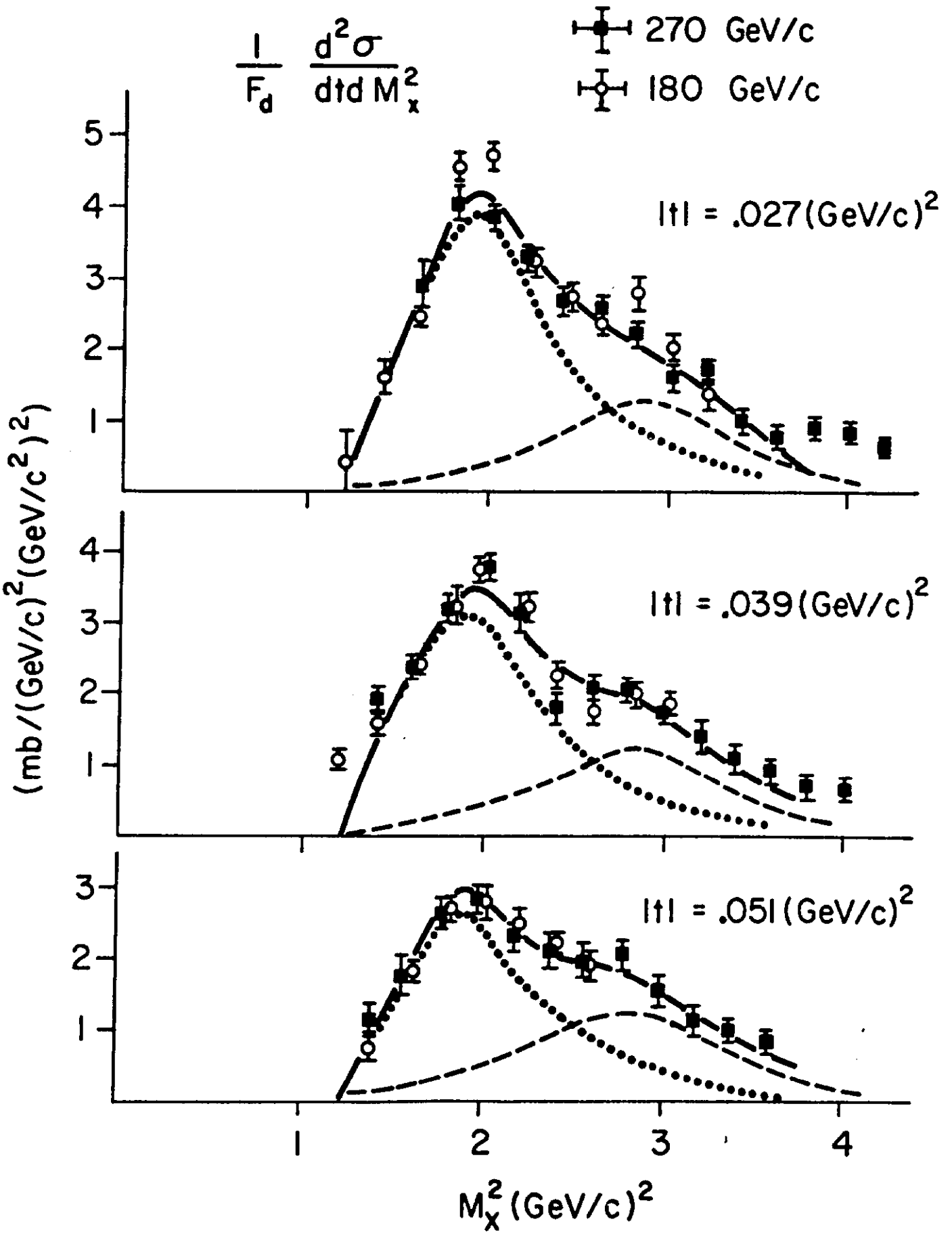
$\frac{1}{F_d}\frac{d^2\sigma}{dt\,dM_x^2}$
270 GeV/c
180 GeV/c
$|t| = .027 (GeV/c)^2$
$|t| = .039 (GeV/c)^2$
$|t| = .051 (GeV/c)^2$
$(mb/(GeV/c)^2 (GeV/c^2)^2)$
$M_x^2 (GeV/c)^2$

FIG. 9

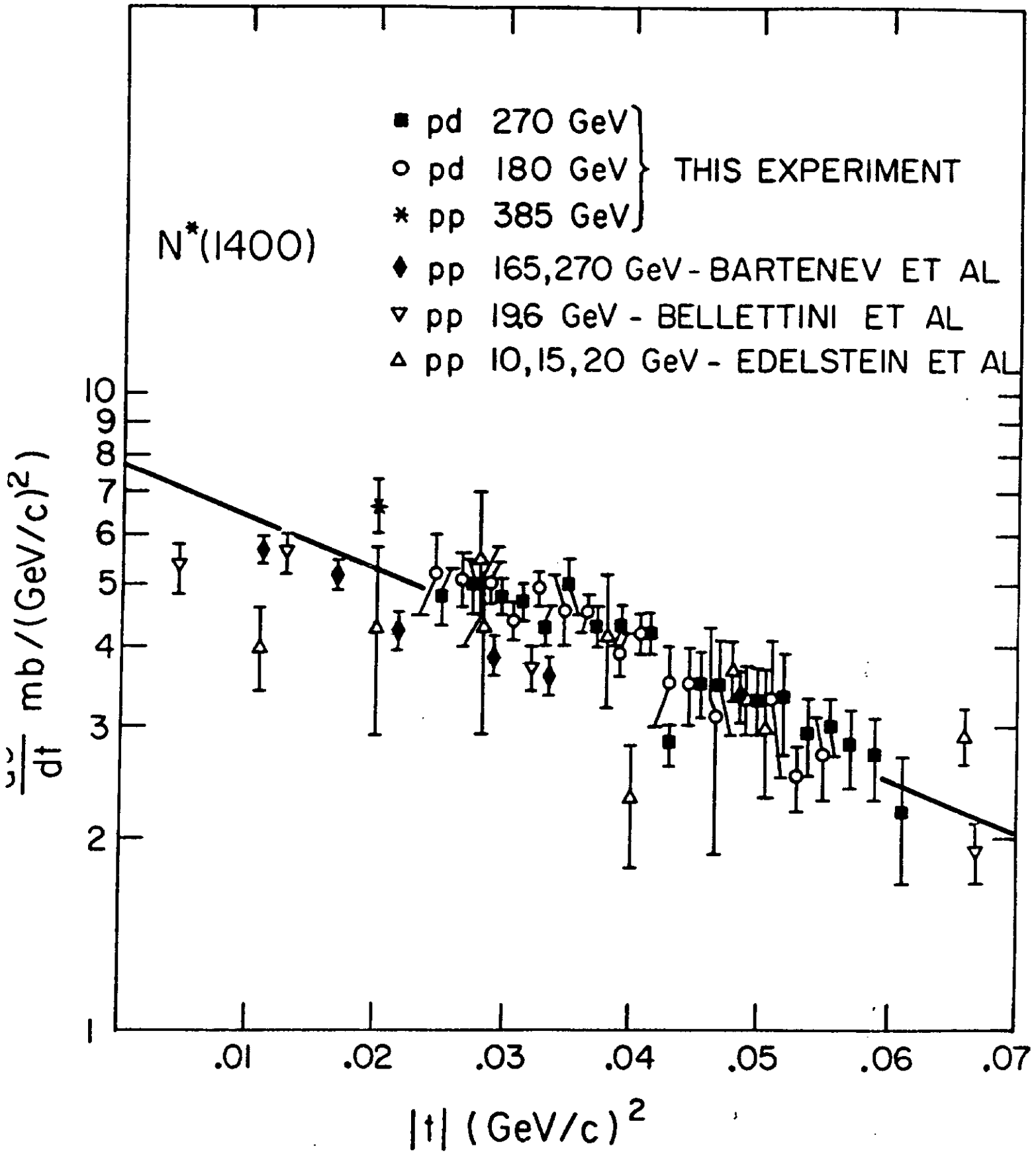
pd 270 GeV
pd 180 GeV
THIS EXPERIMENT
pp 385 GeV
N*(1400)
pp 165,270 GeV - BARTENEV ET AL
pp 19.6 GeV - BELLETTINI ET AL
pp 10,15,20 GeV - EDELSTEIN ET AL
dσ/dt mb/(GeV/c)²
10
9
8
7
6
5
4
3
2
1
.01
.02
.03
.04
.05
.06
.07
|t| (GeV/c)²

FIG. 10

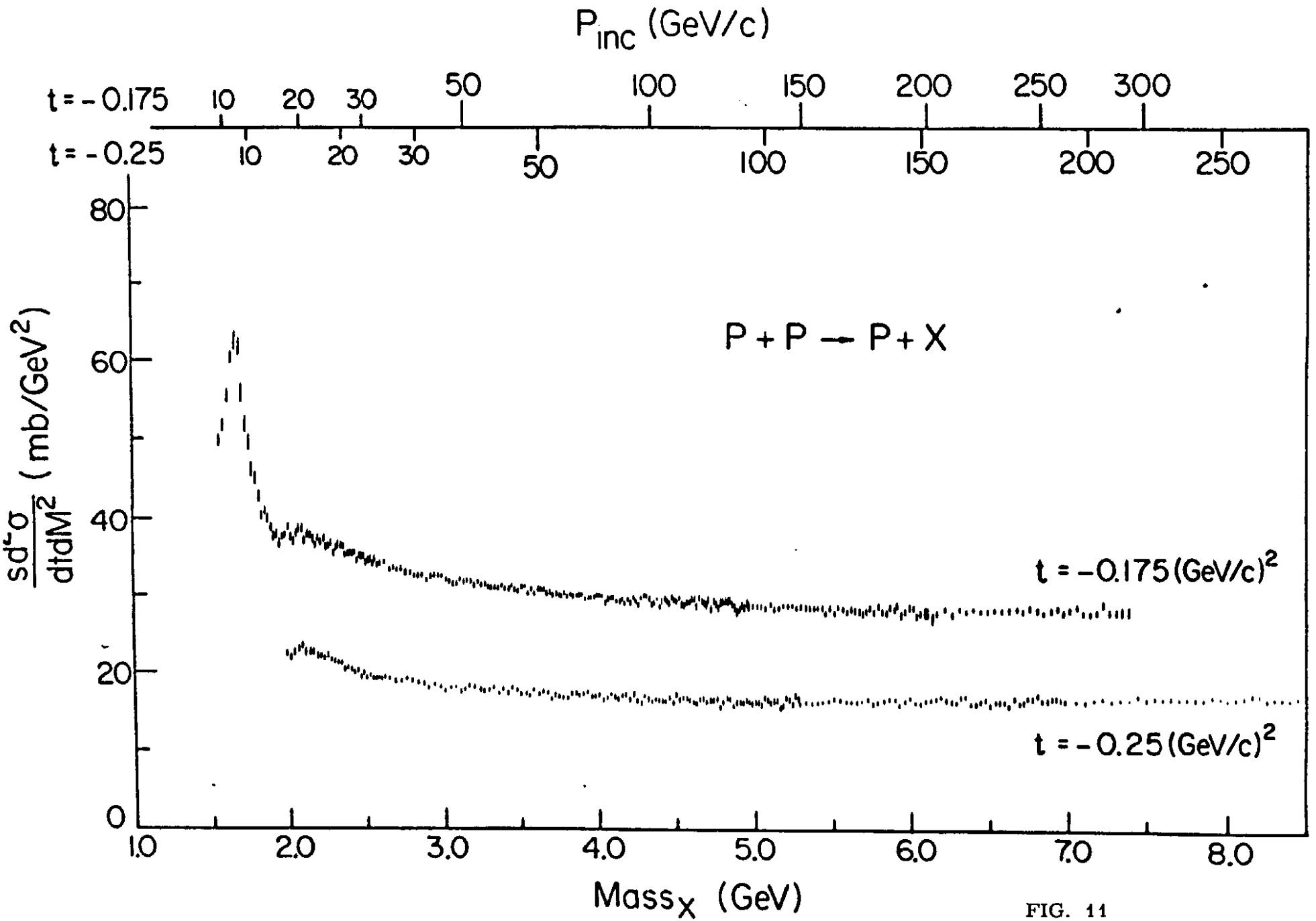
P_inc (GeV/c)
t = -0.175
t = -0.25
10
20
30
50
100
150
200
250
300
80
60
40
20
0
sd²σ / dtdM² (mb/GeV²)
P + P → P + X
t = -0.175 (GeV/c)²
t = -0.25 (GeV/c)²
1.0
2.0
3.0
4.0
5.0
6.0
7.0
8.0
Mass_X (GeV)

FIG. 11

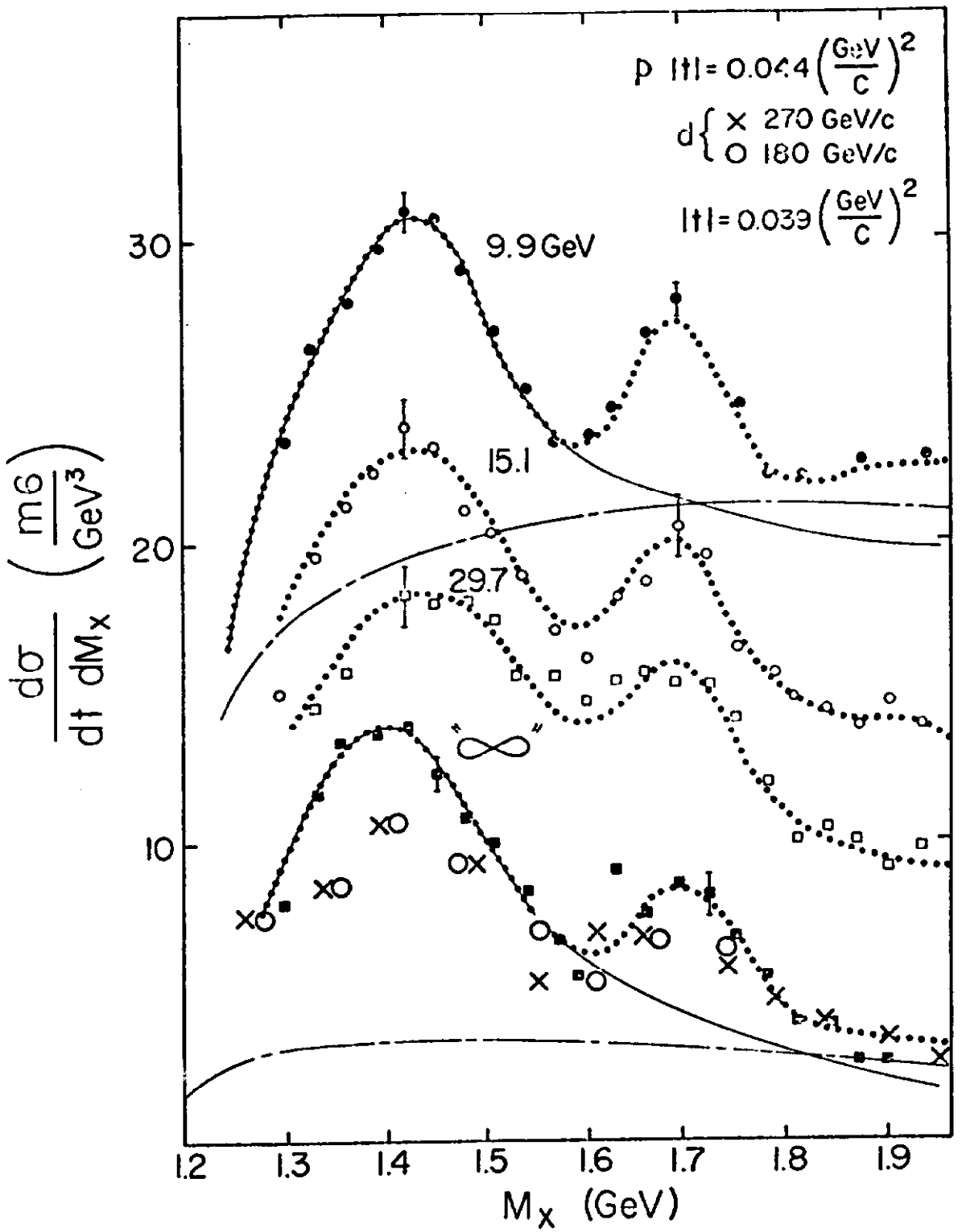
p |t|= 0.044 (GeV/c)²
d { × 270 GeV/c
d { O 180 GeV/c
|t|= 0.039 (GeV/c)²
9.9 GeV
15.1
29.7
dσ/dt dMx (mb/GeV³)
30
20
10
1.2
1.3
1.4
1.5
1.6
1.7
1.8
1.9
Mx (GeV)

FIG. 12

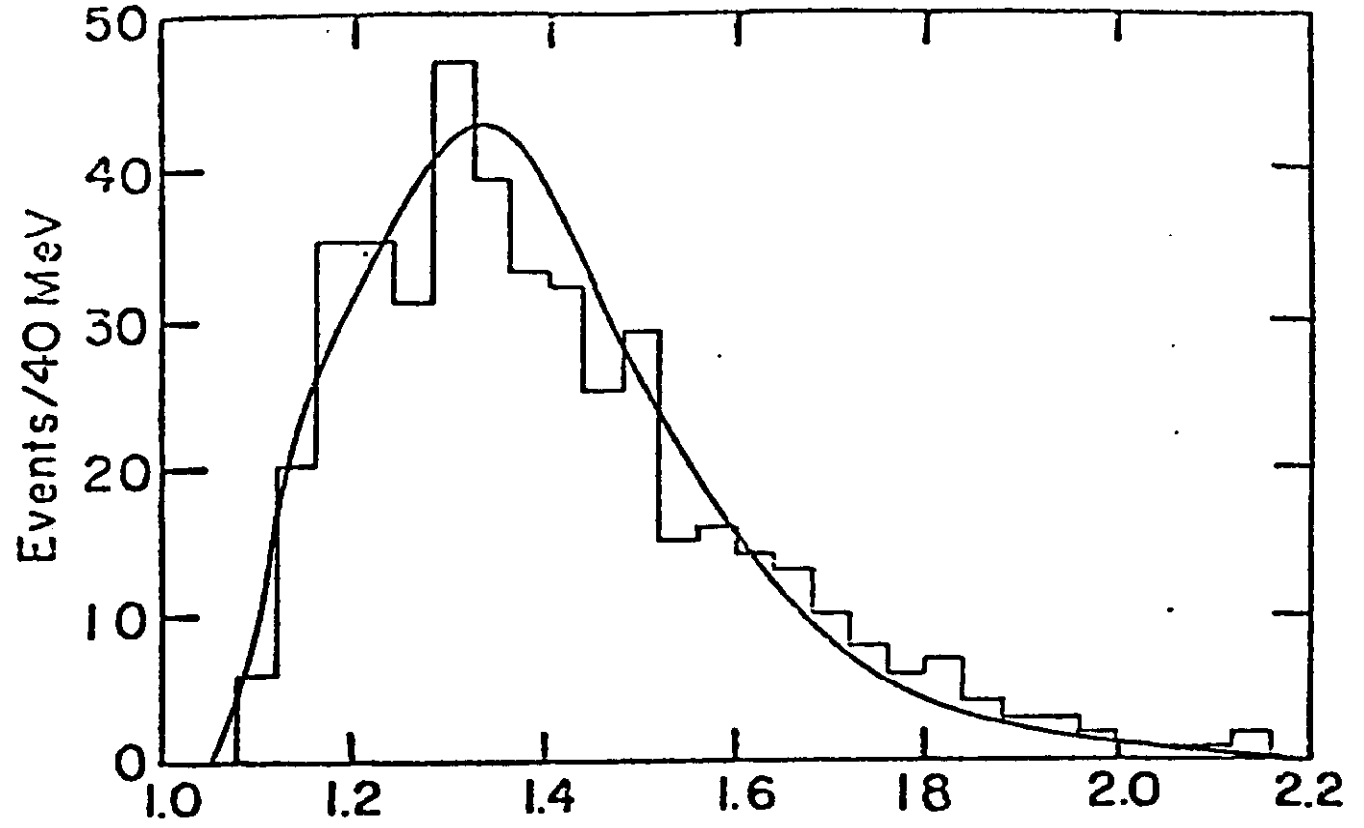
Events/40 MeV
0
10
20
30
40
50
1.0
1.2
1.4
1.6
1.8
2.0
2.2

FIG. 13

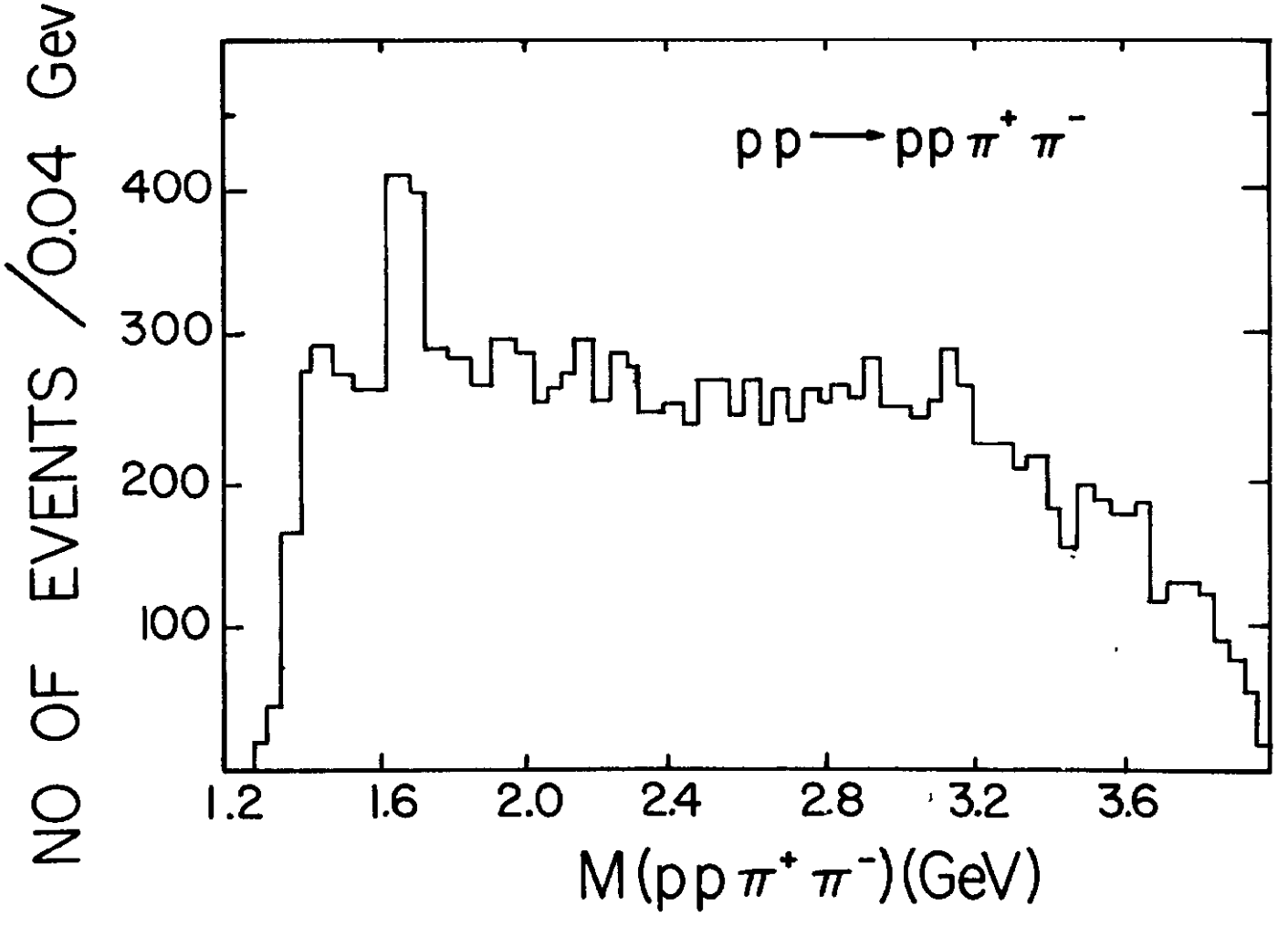
NO OF EVENTS /0.04 Gev
100
200
300
400
1.2
1.6
2.0
2.4
2.8
3.2
3.6
M(pp π⁺ π⁻)(GeV)
pp → pp π⁺ π⁻

FIG. 14

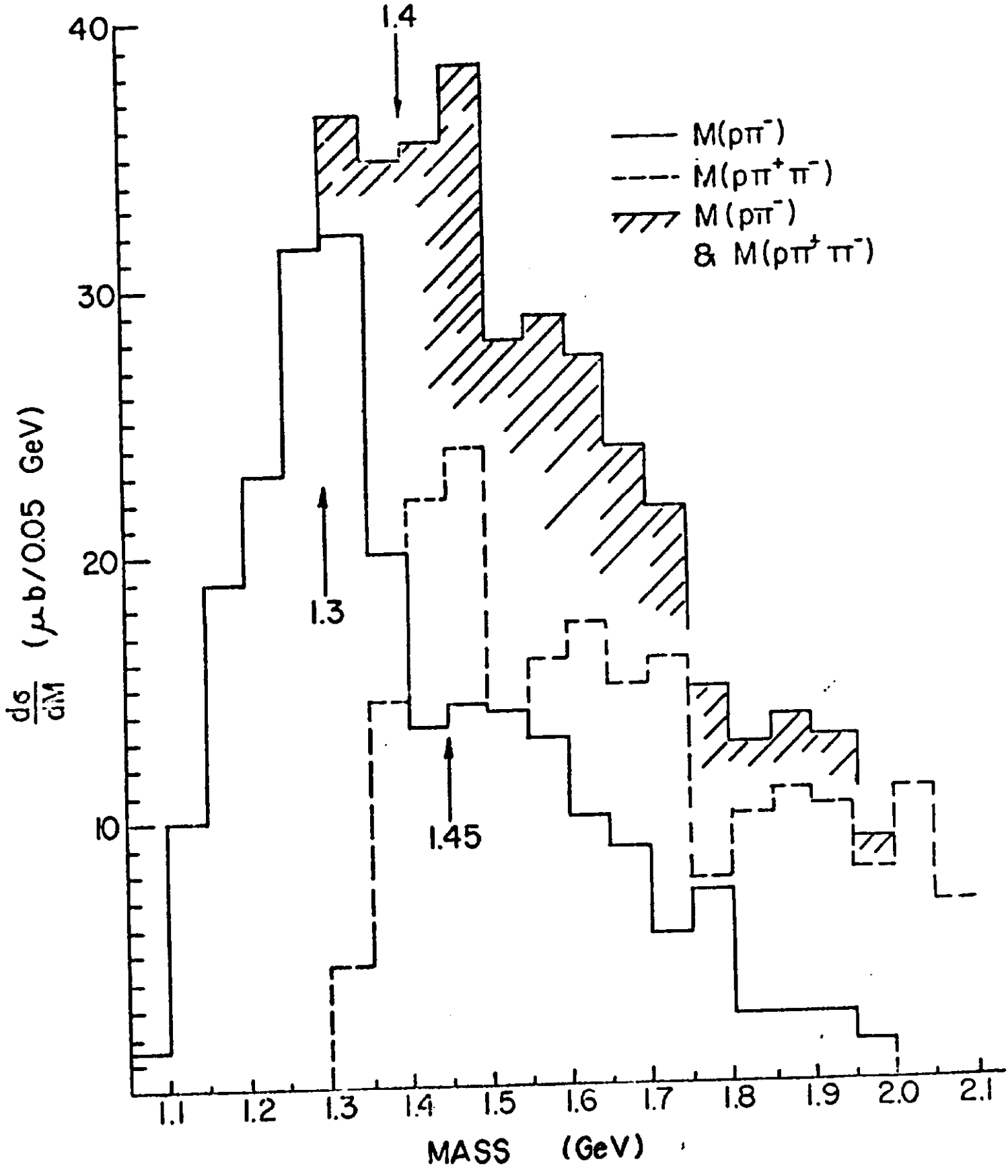
1.4
40
30
20
10
M(pπ⁻)
M(pπ⁺π⁻)
M(pπ⁻)
& M(pπ⁺π⁻)
1.3
1.45
dσ/dM (μb/0.05 GeV)
1.1
1.2
1.3
1.4
1.5
1.6
1.7
1.8
1.9
2.0
2.1
MASS (GeV)

FIG. 15

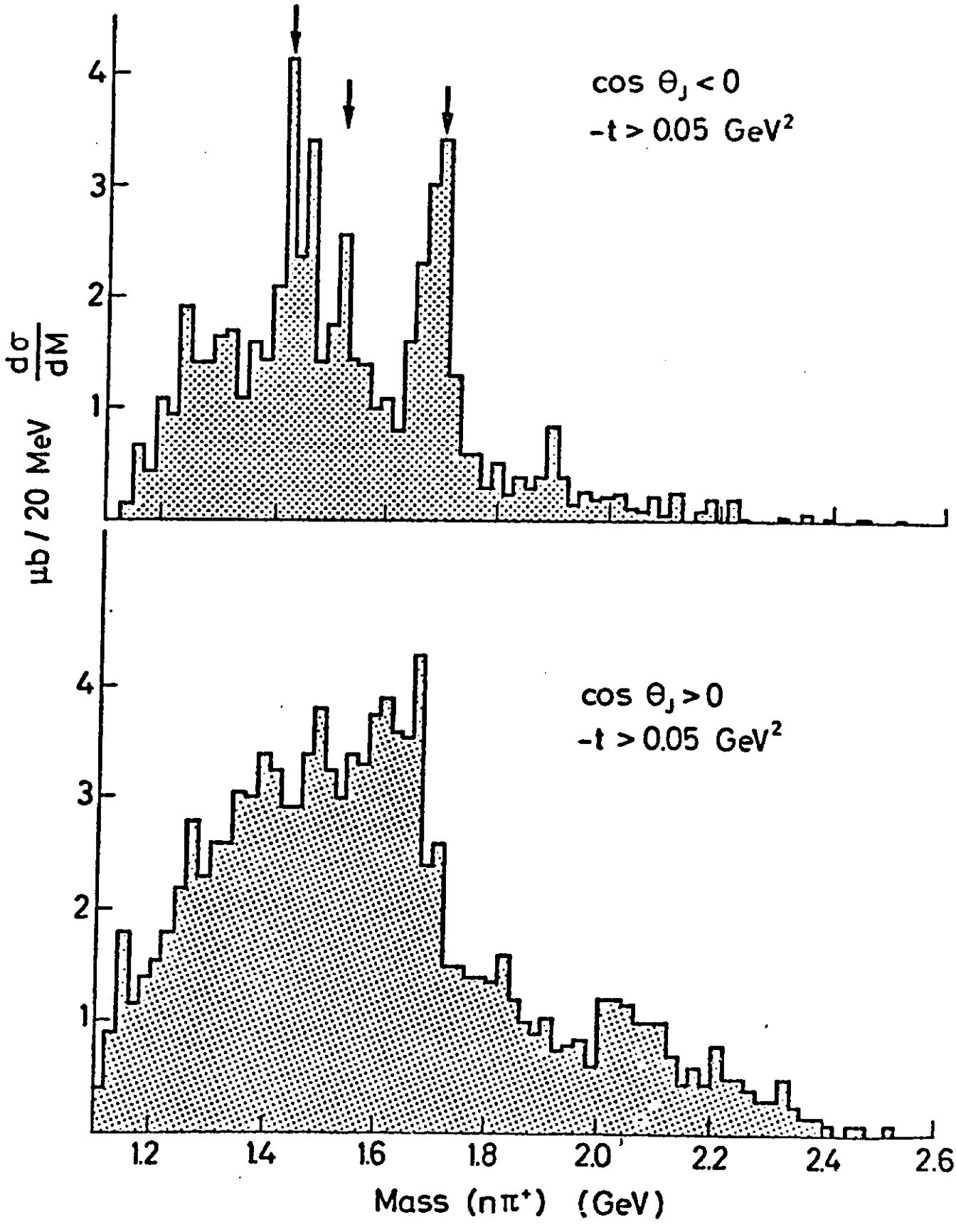
cos θ_J < 0
-t > 0.05 GeV²
cos θ_J > 0
-t > 0.05 GeV²
dσ/dM
μb / 20 MeV
Mass (nπ⁺) (GeV)
1.2
1.4
1.6
1.8
2.0
2.2
2.4
2.6
1
2
3
4

FIG. 16

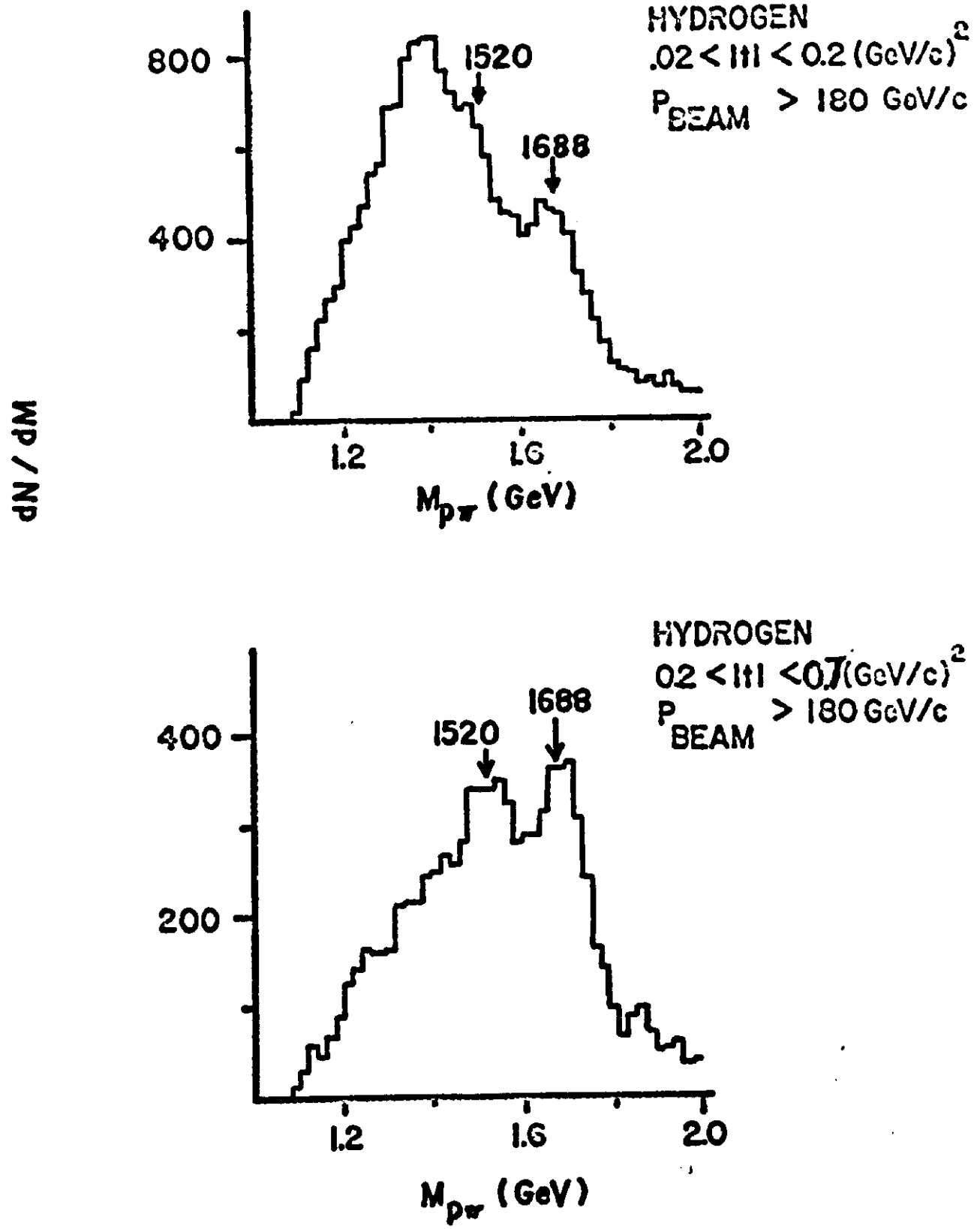
HYDROGEN
.02 < |t| < 0.2 (GeV/c)²
P_BEAM > 180 GeV/c
800
400
1520
1688
1.2
1.6
2.0
M_pπ (GeV)
dN / dM
HYDROGEN
02 < |t| < 0.7 (GeV/c)²
P_BEAM > 180 GeV/c
400
200
1520
1688
1.2
1.6
2.0
M_pπ (GeV)

FIG. 17

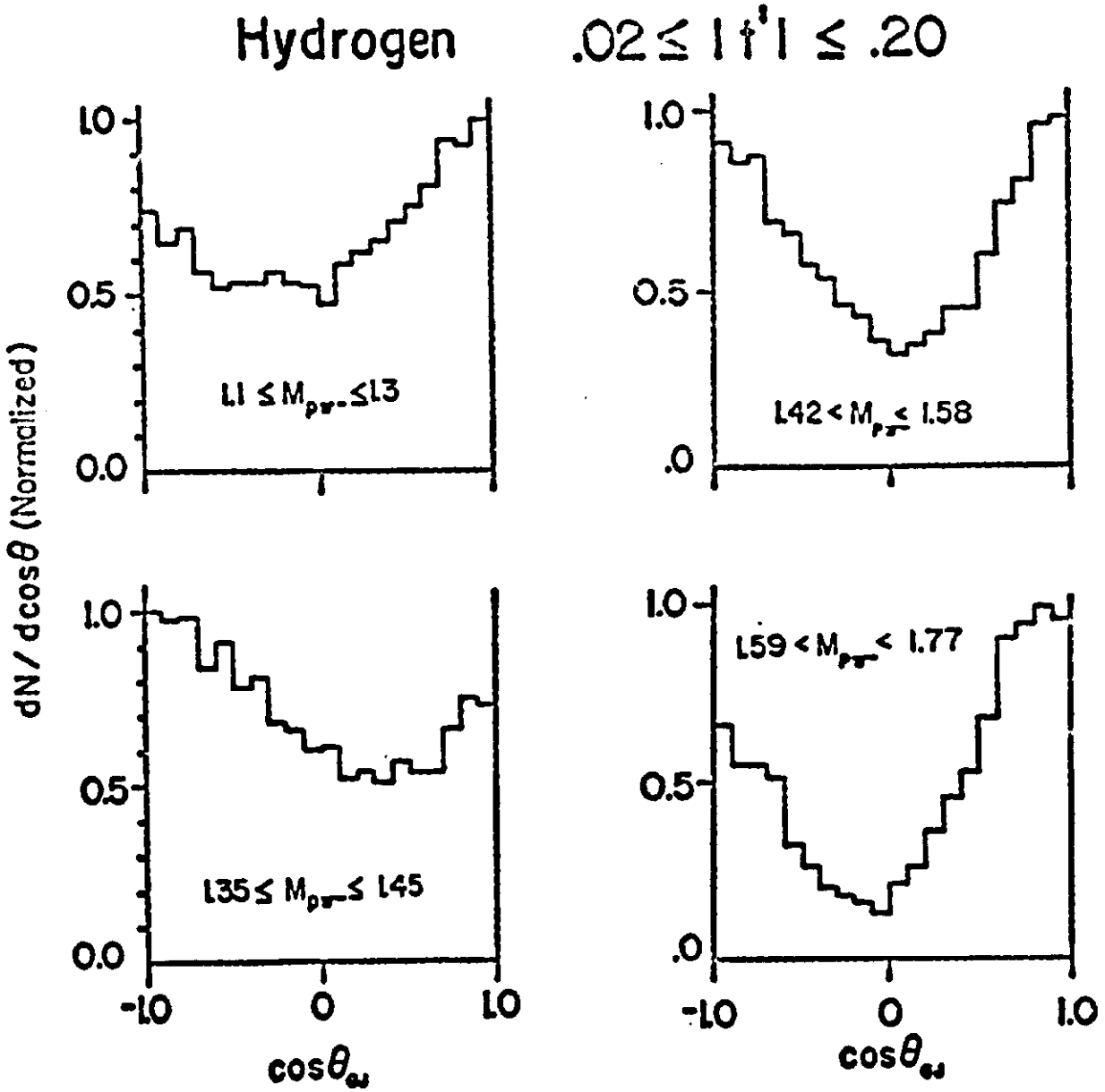
Hydrogen
.02 ≤ |t'| ≤ .20
dN / dcosθ (Normalized)
1.0
0.5
0.0
1.1 ≤ M_pπ- ≤ 1.3
1.42 < M_pπ- ≤ 1.58
.0
1.35 ≤ M_pπ- ≤ 1.45
1.59 < M_pπ- < 1.77
-1.0
0
1.0
cosθ_GJ

FIG. 18

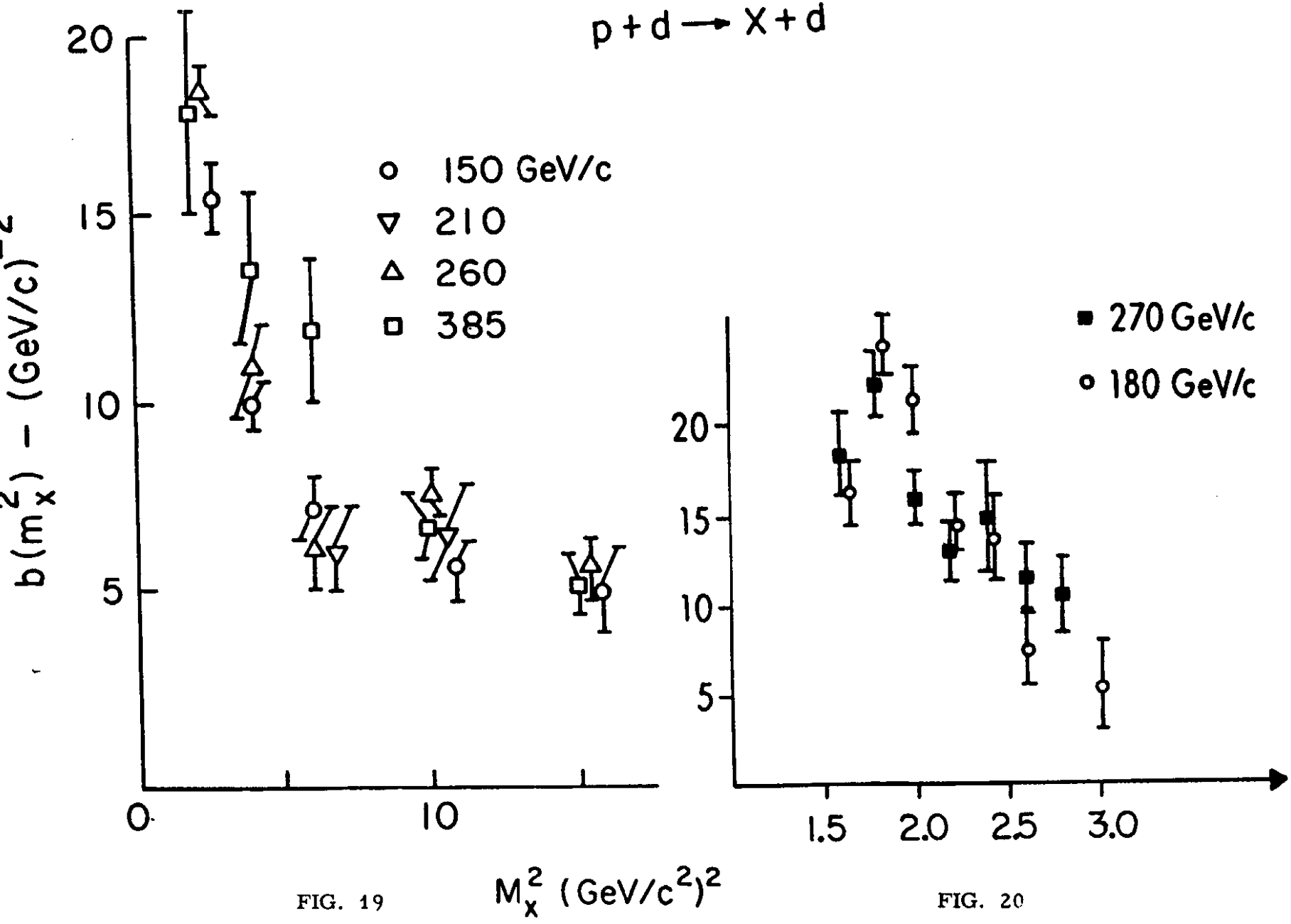
p + d → X + d
150 GeV/c
210
260
385
270 GeV/c
180 GeV/c
$b(m_x^2) - (GeV/c)^{-2}$
M_x^2 $(GeV/c^2)^2$
0
10
20
5
15
1.5
2.0
2.5
3.0

FIG. 19

FIG. 20

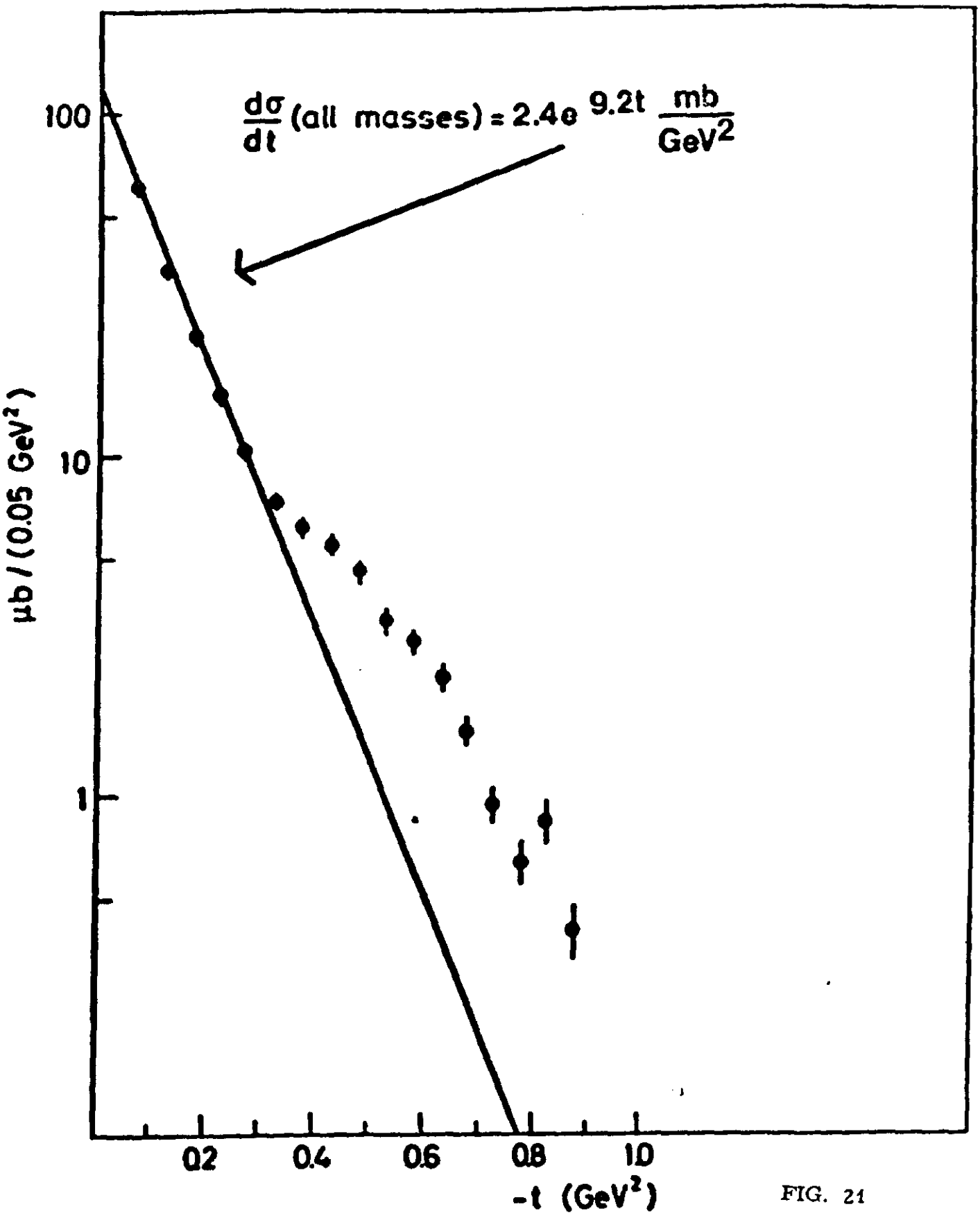
$\frac{d\sigma}{dt}$ (all masses) = 2.4e$^{9.2t}$ $\frac{mb}{GeV^2}$
100
10
1
μb / (0.05 GeV²)
0.2
0.4
0.6
0.8
1.0
-t (GeV²)

FIG. 21

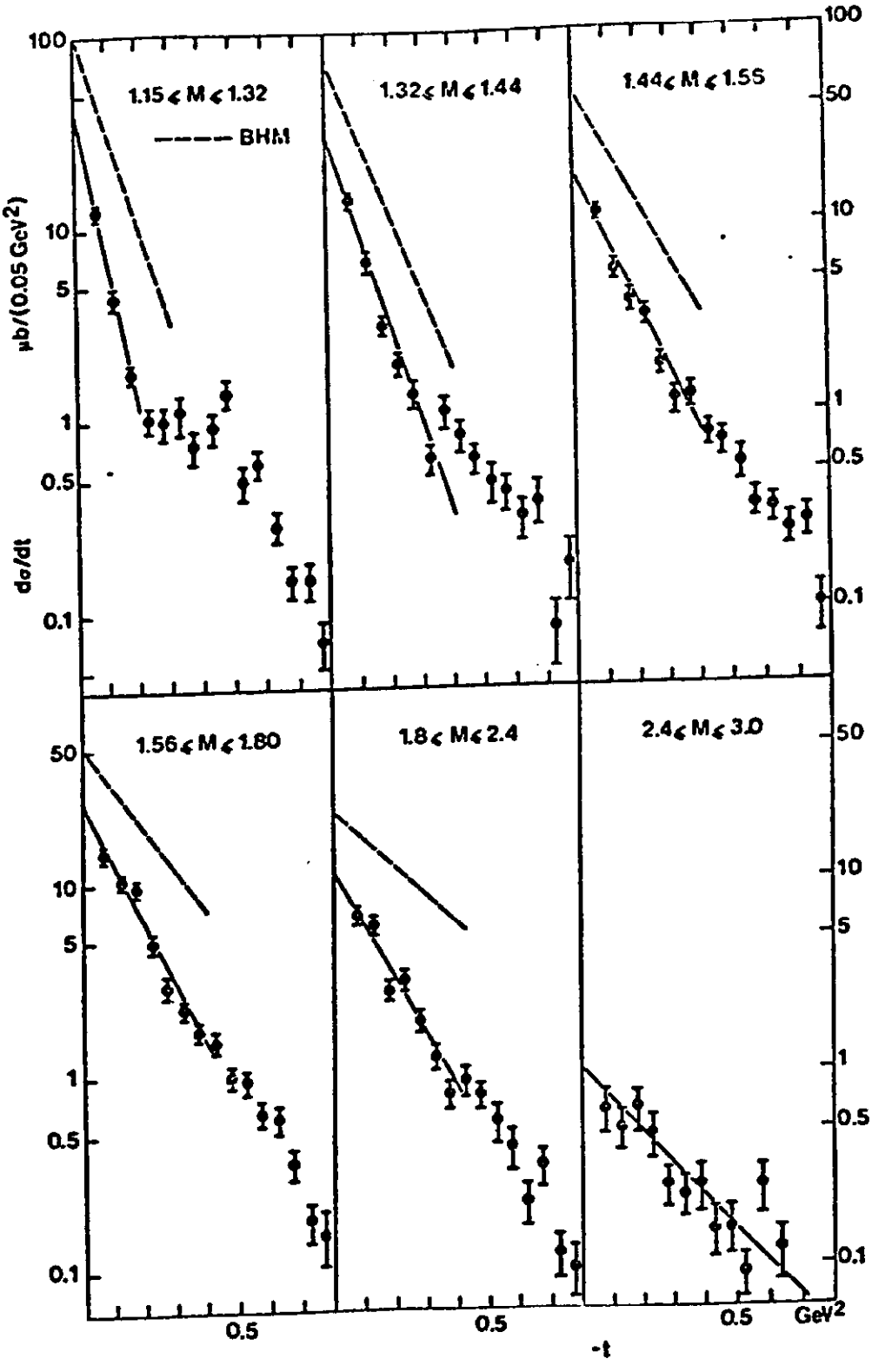
1.15 < M < 1.32
BHM
1.32 < M < 1.44
1.44 < M < 1.55
1.56 < M < 1.80
1.8 < M < 2.4
2.4 < M < 3.0
μb/(0.05 GeV²)
dσ/dt
-t
GeV²

FIG. 22

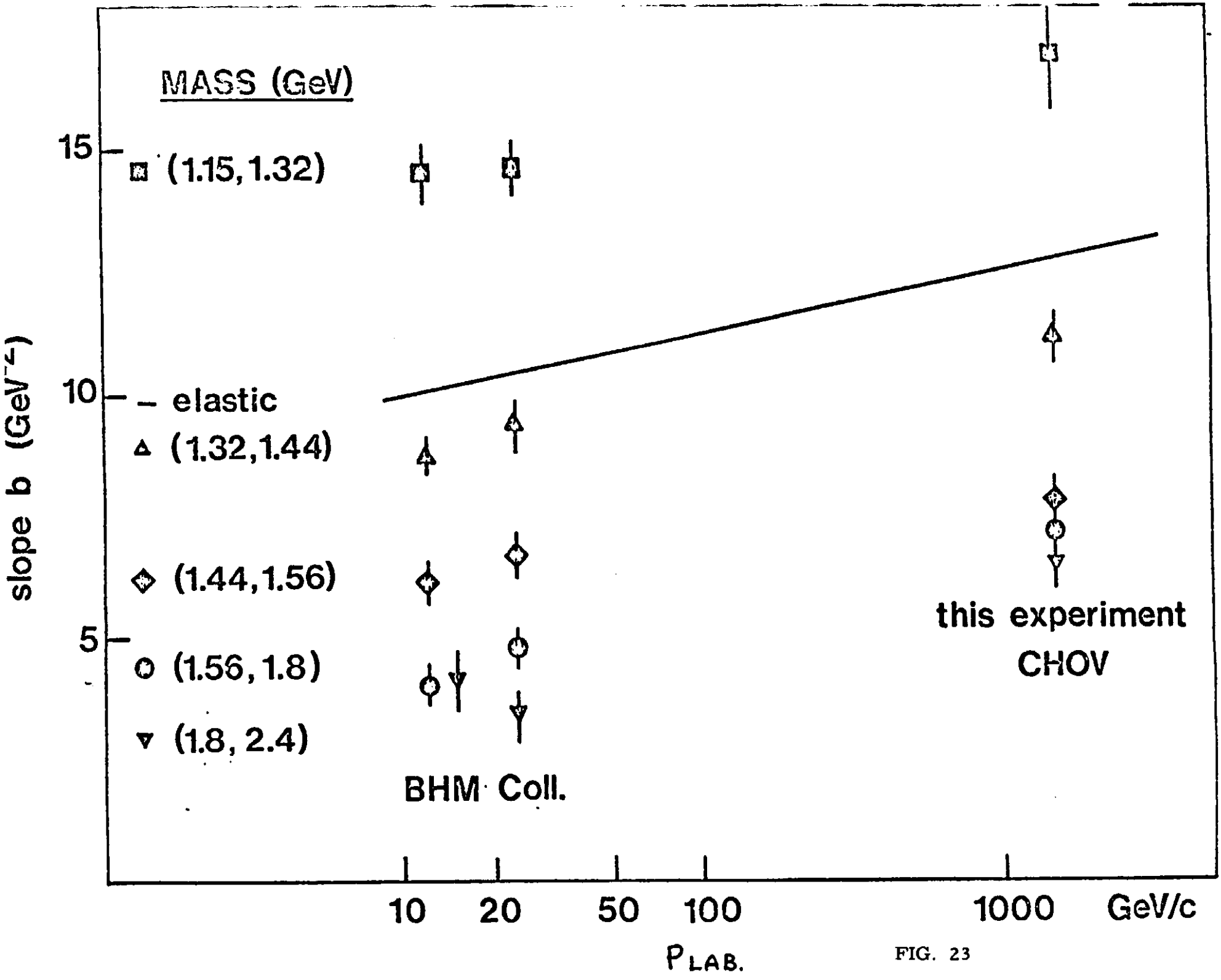
MASS (GeV)
(1.15, 1.32)
elastic
(1.32, 1.44)
(1.44, 1.56)
(1.56, 1.8)
(1.8, 2.4)
BHM Coll.
this experiment
CHOV
slope b (GeV⁻²)
15
10
5
10
20
50
100
1000
GeV/c
P LAB.

FIG. 23

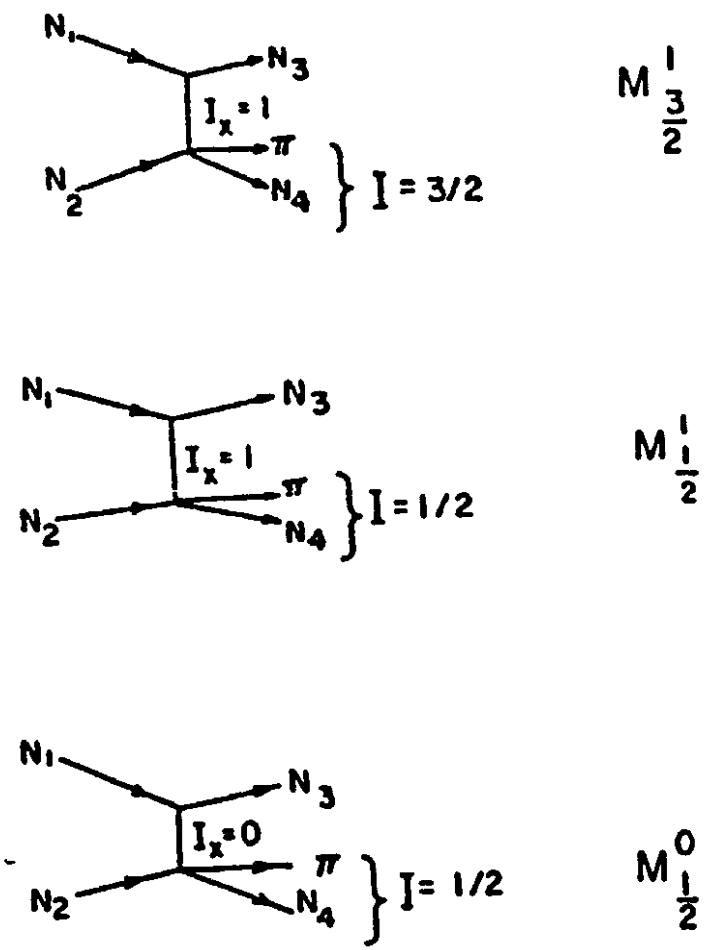
N1
N3
Ix = 1
π
N2
N4
I = 3/2
M 3/2 I
N1
N3
Ix = 1
π
N2
N4
I = 1/2
M 1/2 I
N1
N3
Ix = 0
π
N2
N4
I = 1/2
M 1/2 0

FIG. 24

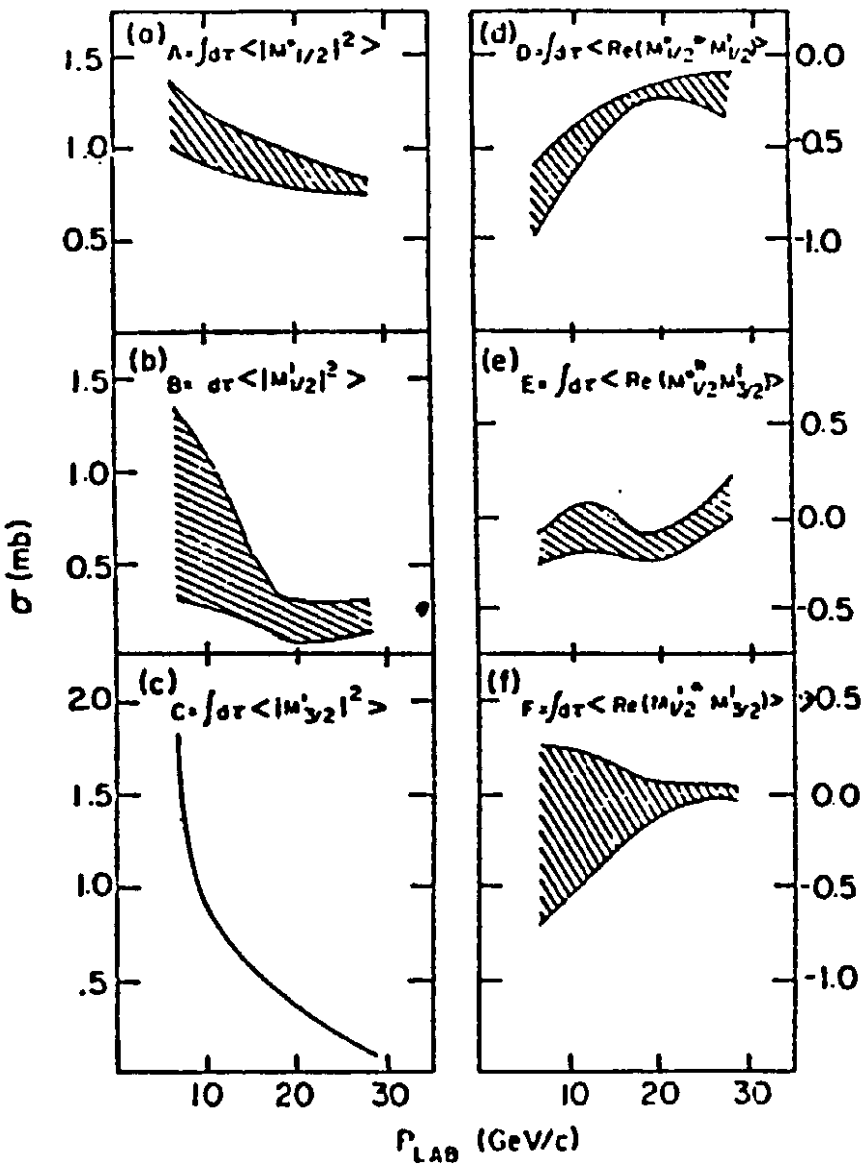
(a) A = ∫dτ < |M*1/2|² >
(b) B = ∫dτ < |M'1/2|² >
(c) C = ∫dτ < |M'3/2|² >
(d) D = ∫dτ < Re(M*1/2 M'1/2) >
(e) E = ∫dτ < Re(M*1/2 M'3/2) >
(f) F = ∫dτ < Re(M'*1/2 M'3/2) >
σ (mb)
P LAB (GeV/c)

FIG. 25

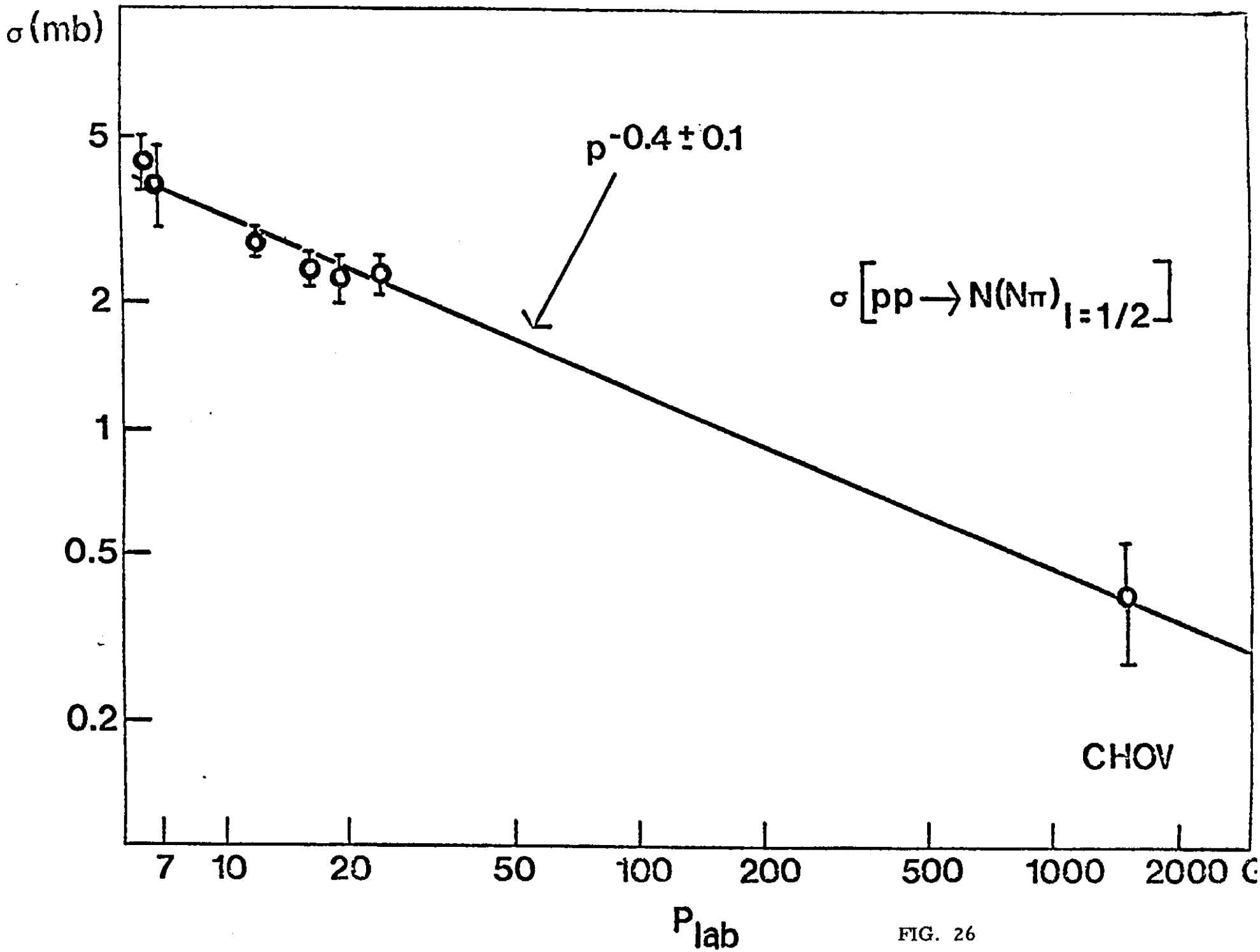
σ (mb)
5
2
1
0.5
0.2
p^-0.4 ± 0.1
σ [pp → N(Nπ)I=1/2]
CHOV
7
10
20
50
100
200
500
1000
2000
Plab

FIG. 26

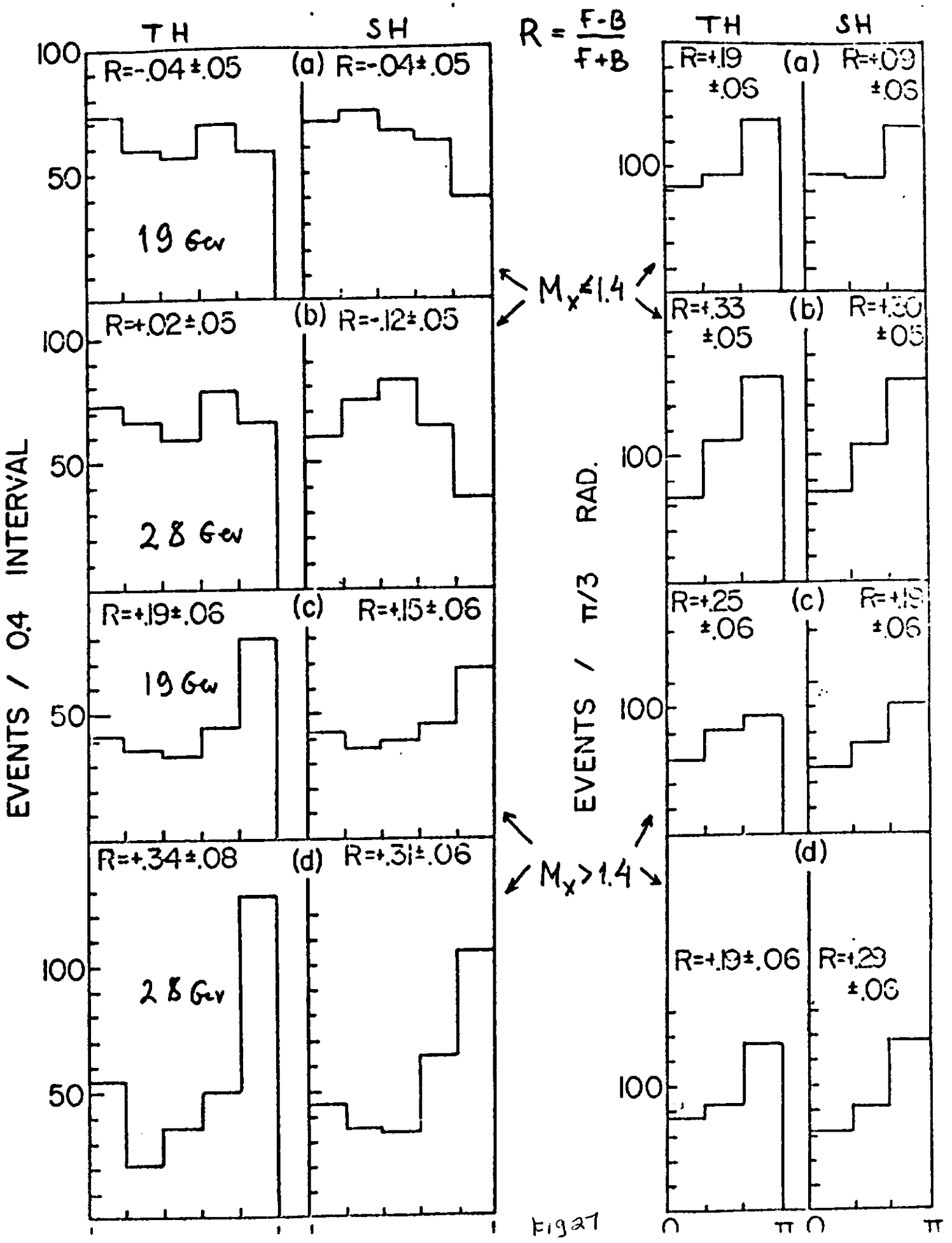
TH
SH
$R = \frac{F-B}{F+B}$
TH
SH
R=-.04±.05
(a) R=-.04±.05
R=+.19 ±.06
(a) R=+.09 ±.06
19 Gev
$M_x \leq 1.4$
R=+.02±.05
(b) R=-.12±.05
R=+.33 ±.05
(b) R=+.30 ±.05
2.8 Gev
R=+.19±.06
(c) R=+.15±.06
R=+.25 ±.06
(c) R=+.15 ±.06
19 Gev
$M_x > 1.4$
R=+.34±.08
(d) R=+.31±.06
(d)
R=+.19±.06
R=+.23 ±.06
2.8 Gev
EVENTS / 0.4 INTERVAL
EVENTS / π/3 RAD.
100
50
0
π

Figa1

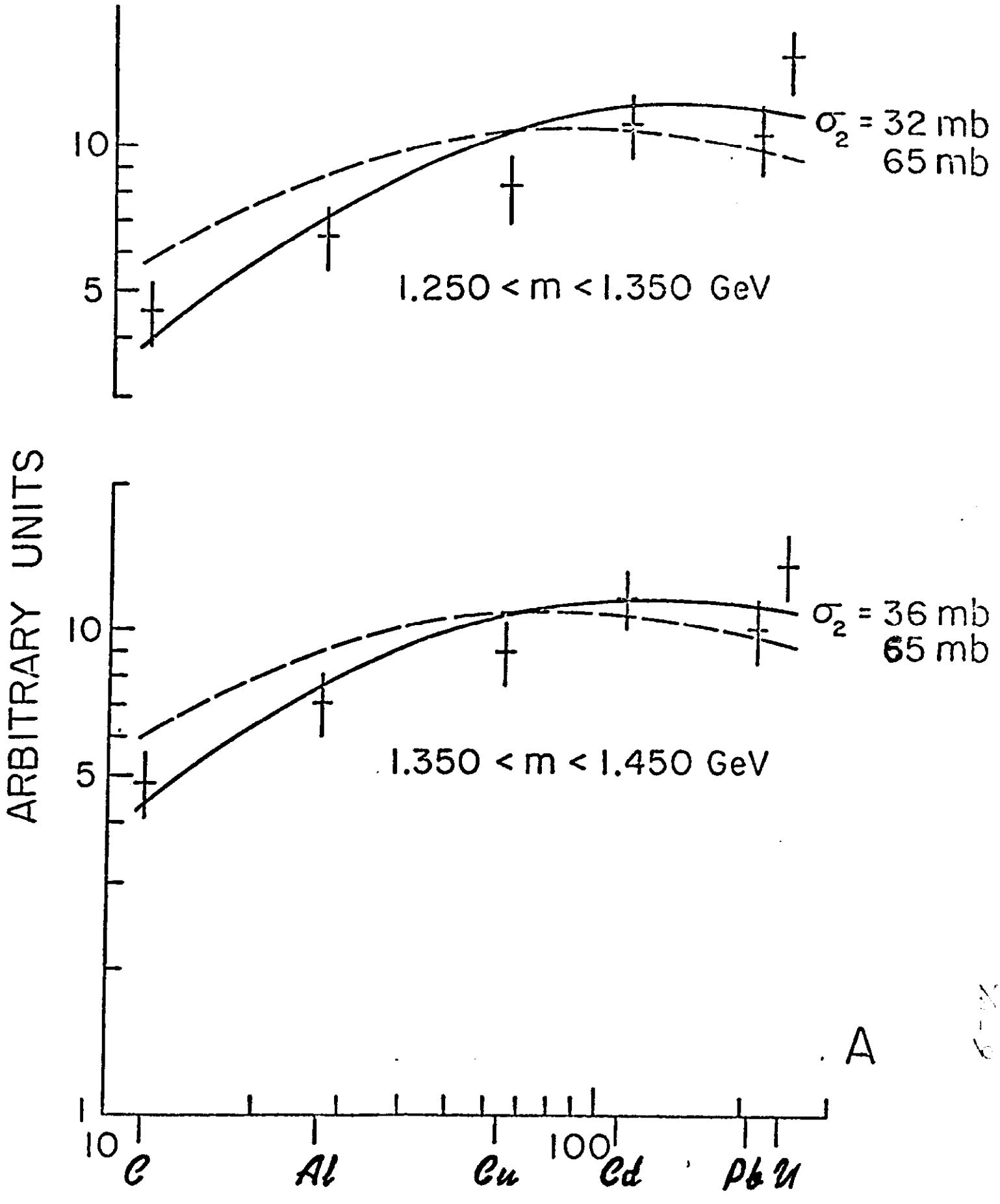
ARBITRARY UNITS
10
5
1
σ_2 = 32 mb
65 mb
1.250 < m < 1.350 GeV
σ_2 = 36 mb
65 mb
1.350 < m < 1.450 GeV
A
10
C
Al
Cu
100
Cd
Pb U

FIG. 28

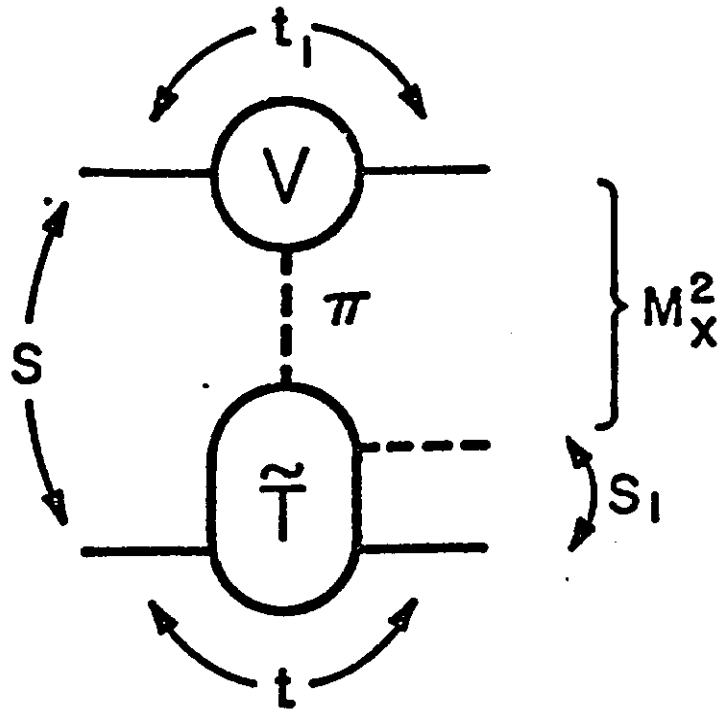

(a)

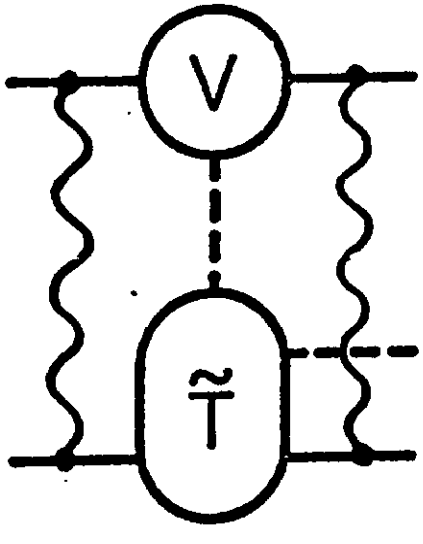

(b)

FIG. 29

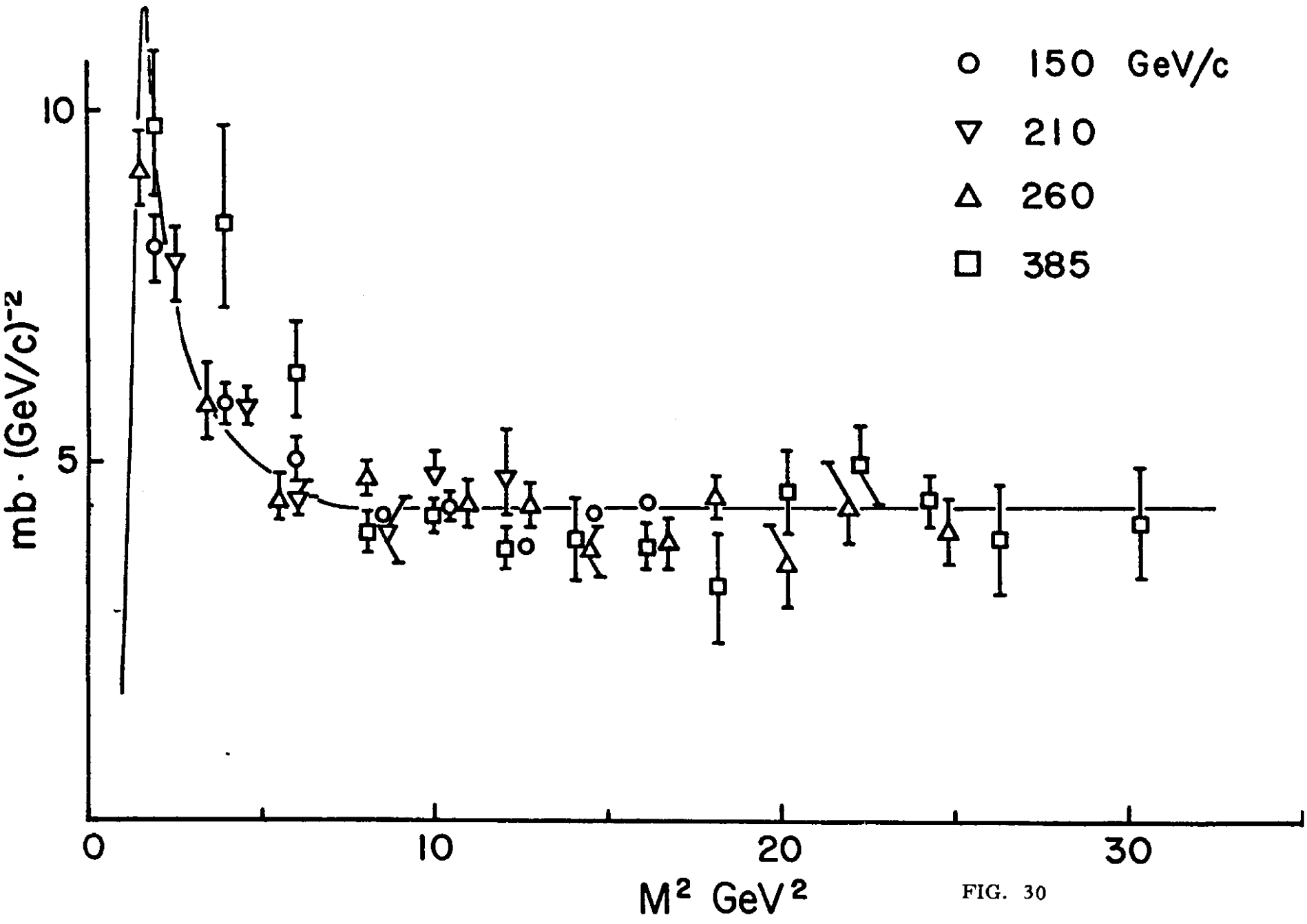
$M^2 \frac{1}{F_d(t)} \frac{d^2\sigma}{dt\, dM^2} (pd \to Xd)_{t=0}$
150 GeV/c
210
260
385
mb · (GeV/c)$^{-2}$
10
5
0
10
20
30
M² GeV²

FIG. 30

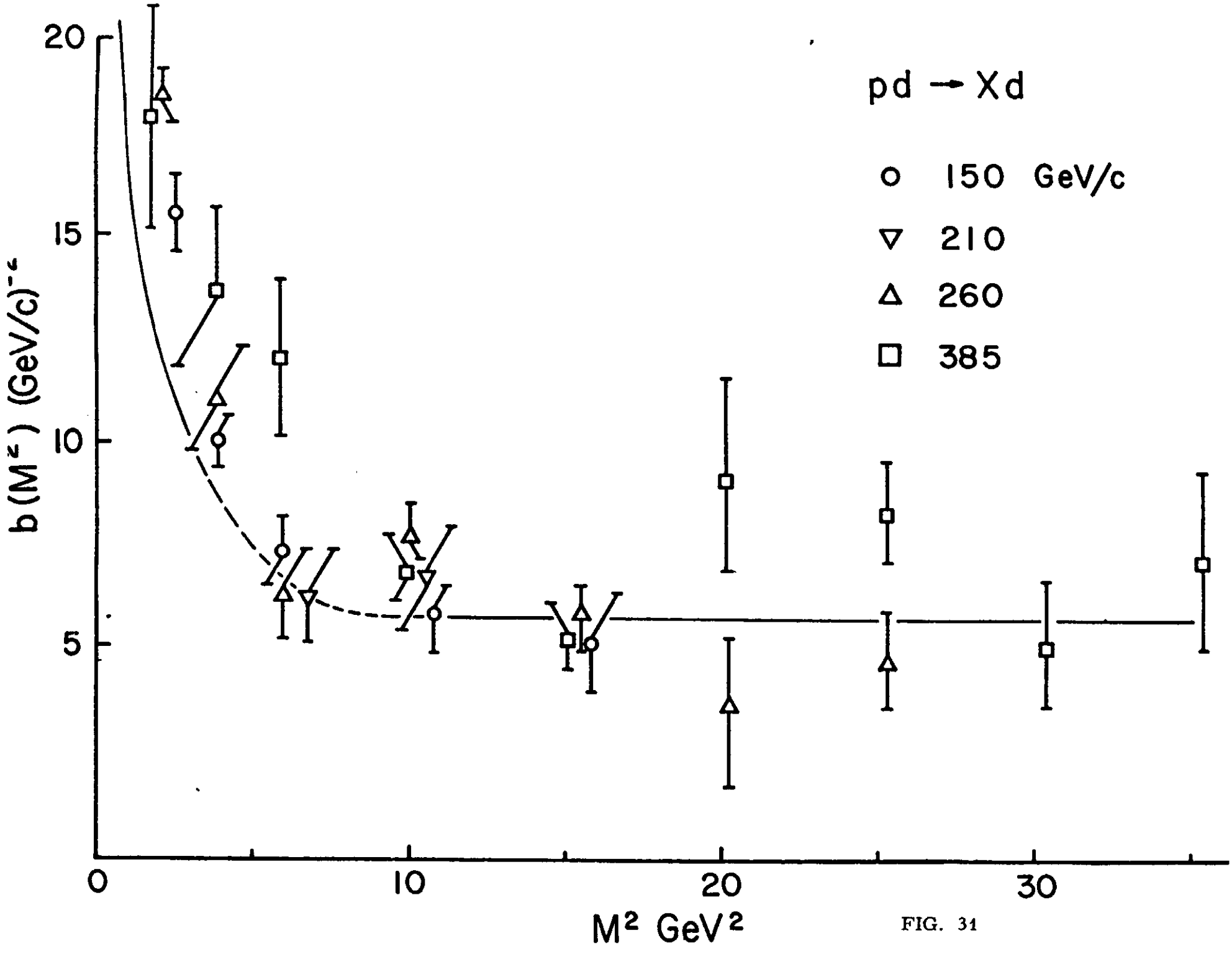

FIG. 31

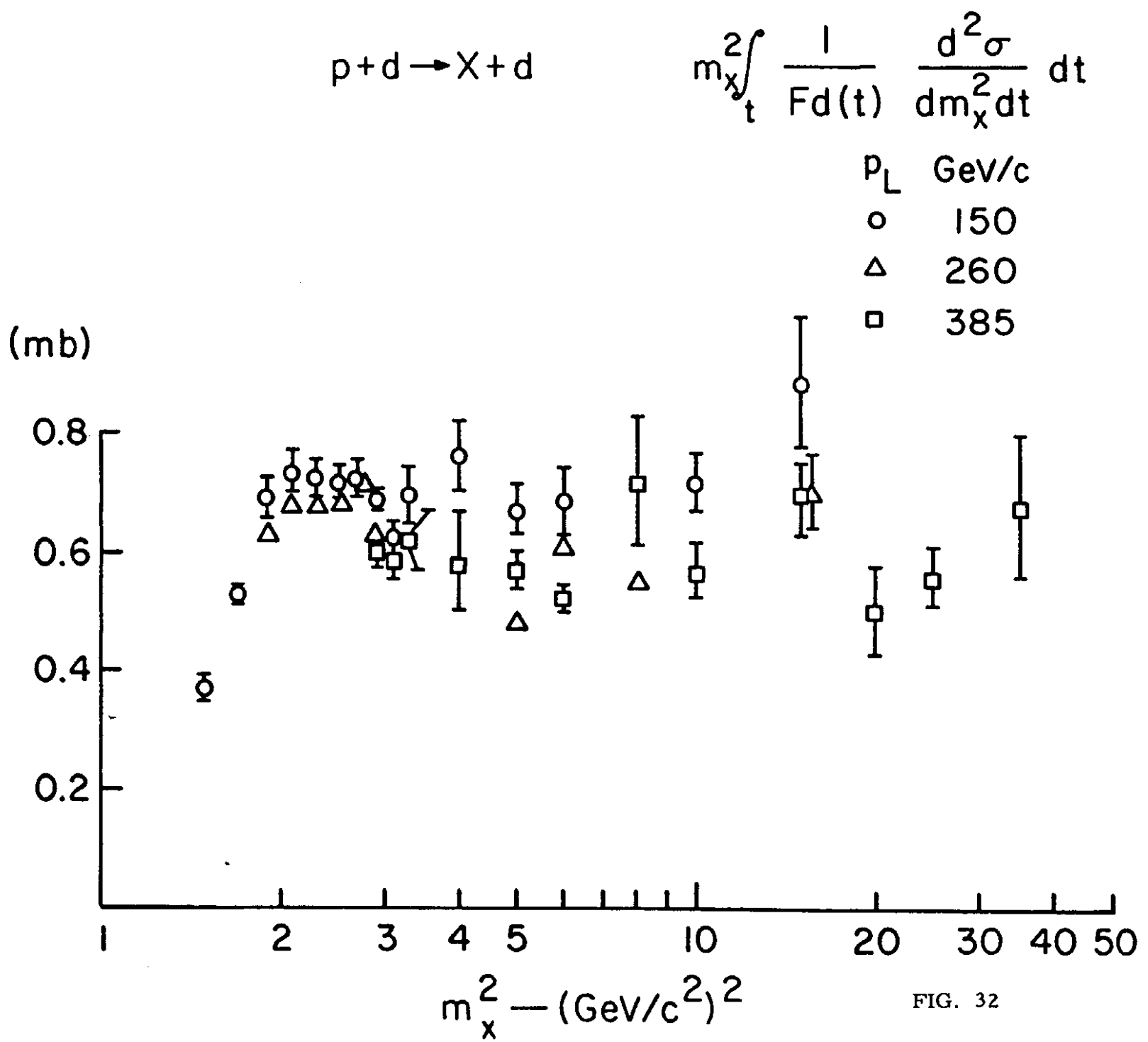
p+d → X+d
$m_x^2 \int_t \frac{1}{Fd(t)} \frac{d^2\sigma}{dm_x^2 dt} dt$
p_L GeV/c
o 150
△ 260
□ 385
(mb)
0.8
0.6
0.4
0.2
1
2
3
4
5
10
20
30
40
50
m_x^2 — (GeV/c^2)^2

FIG. 32

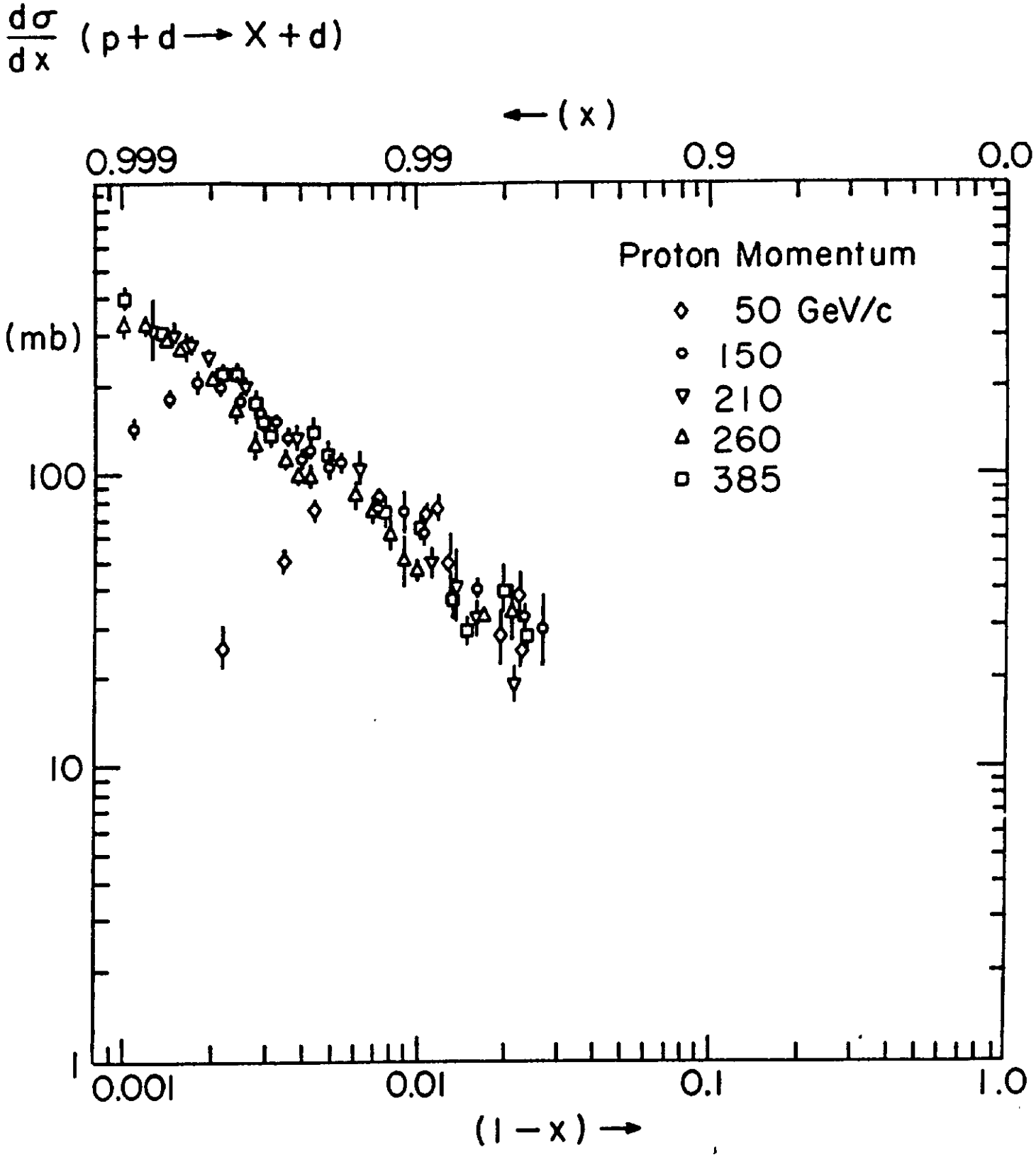
dσ/dx (p+d → X+d)
← (x)
0.999
0.99
0.9
0.0
(mb)
100
10
1
Proton Momentum
50 GeV/c
150
210
260
385
0.001
0.01
0.1
1.0
(1 − x) →

FIG. 33

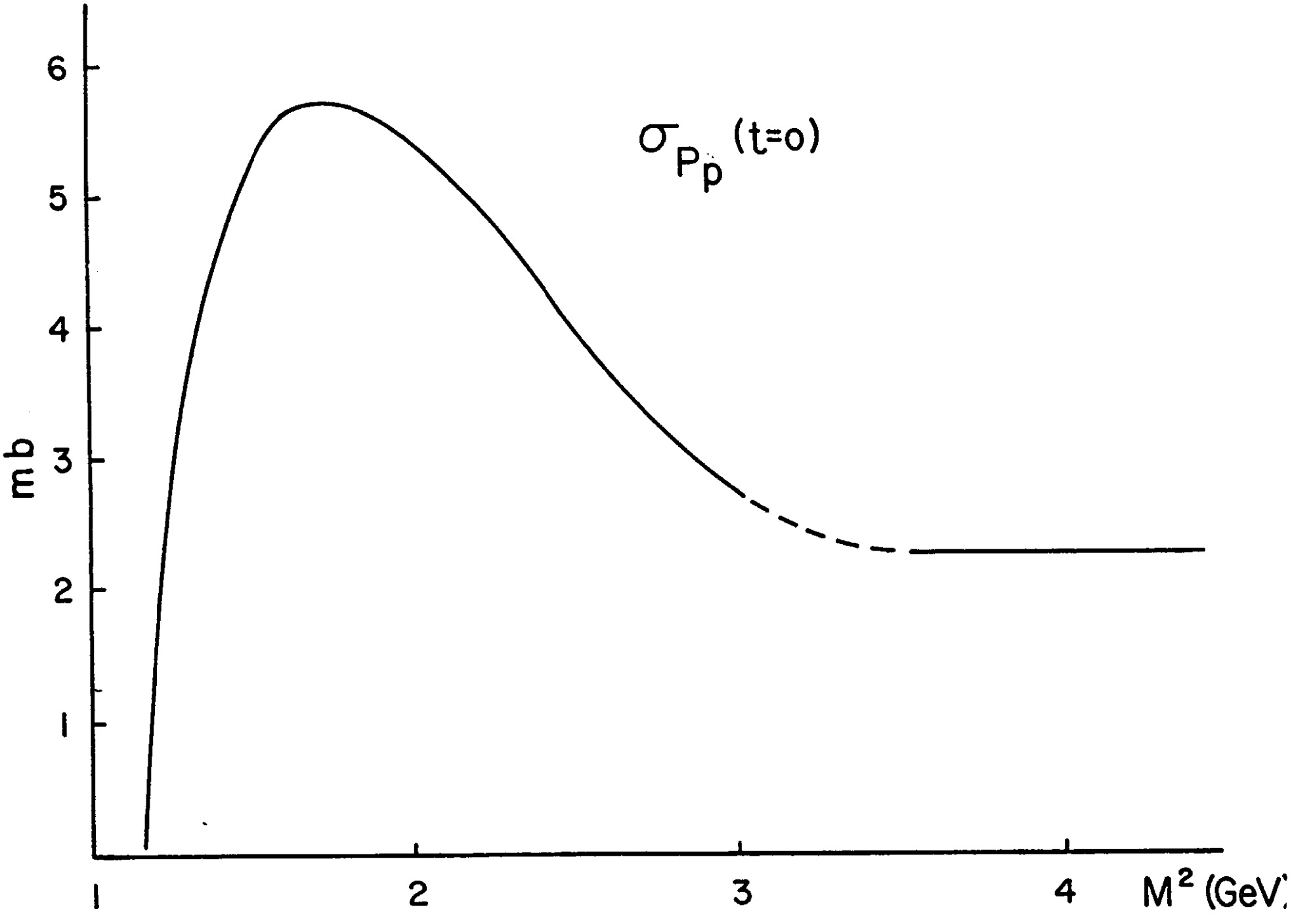

FIG. 34

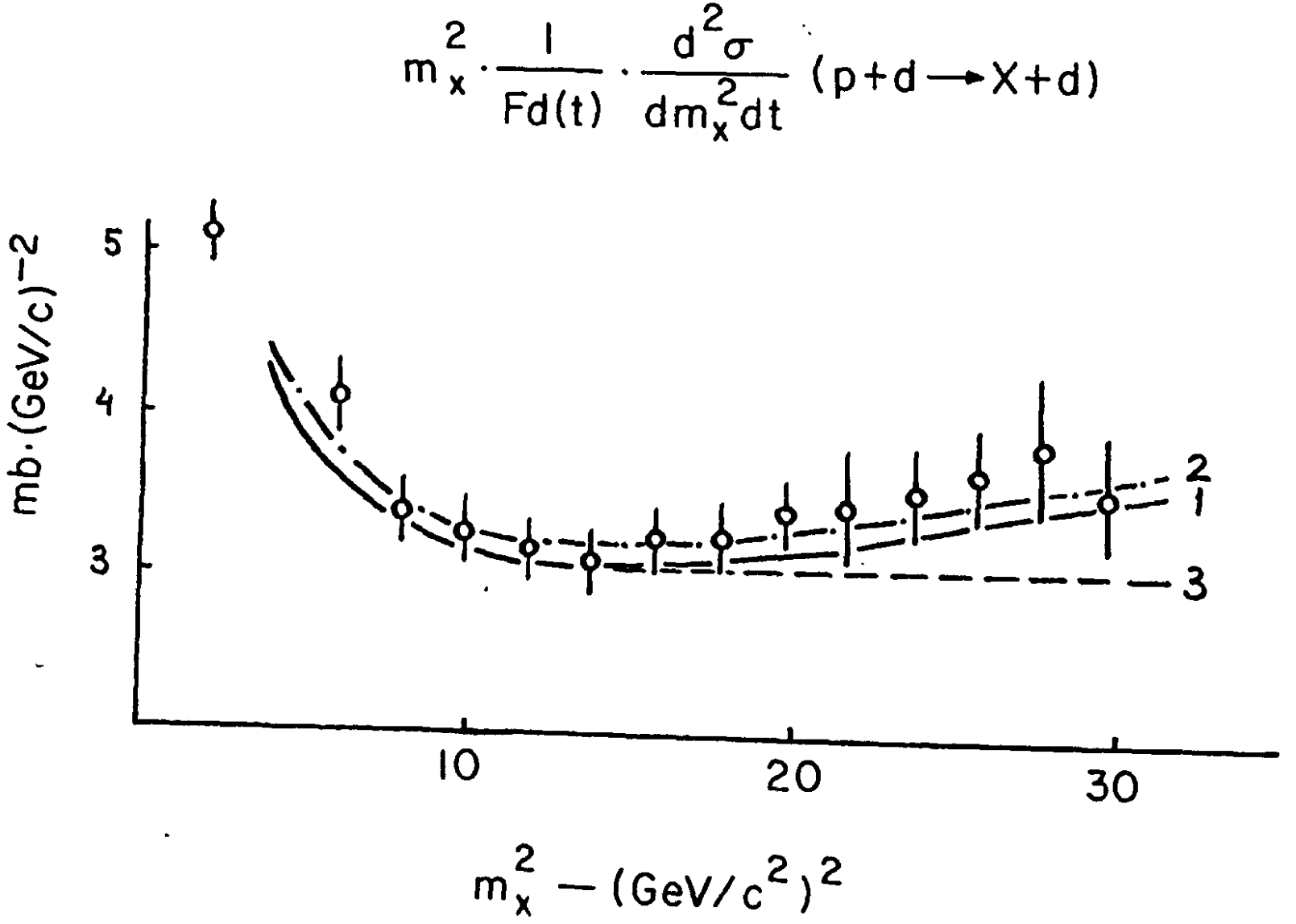
$m_x^2 \cdot \frac{1}{Fd(t)} \cdot \frac{d^2\sigma}{dm_x^2 dt}$ (p+d → X+d)
mb·(GeV/c)$^{-2}$
5
4
3
10
20
30
2
1
3
m_x^2 — (GeV/c^2)^2

FIG. 35

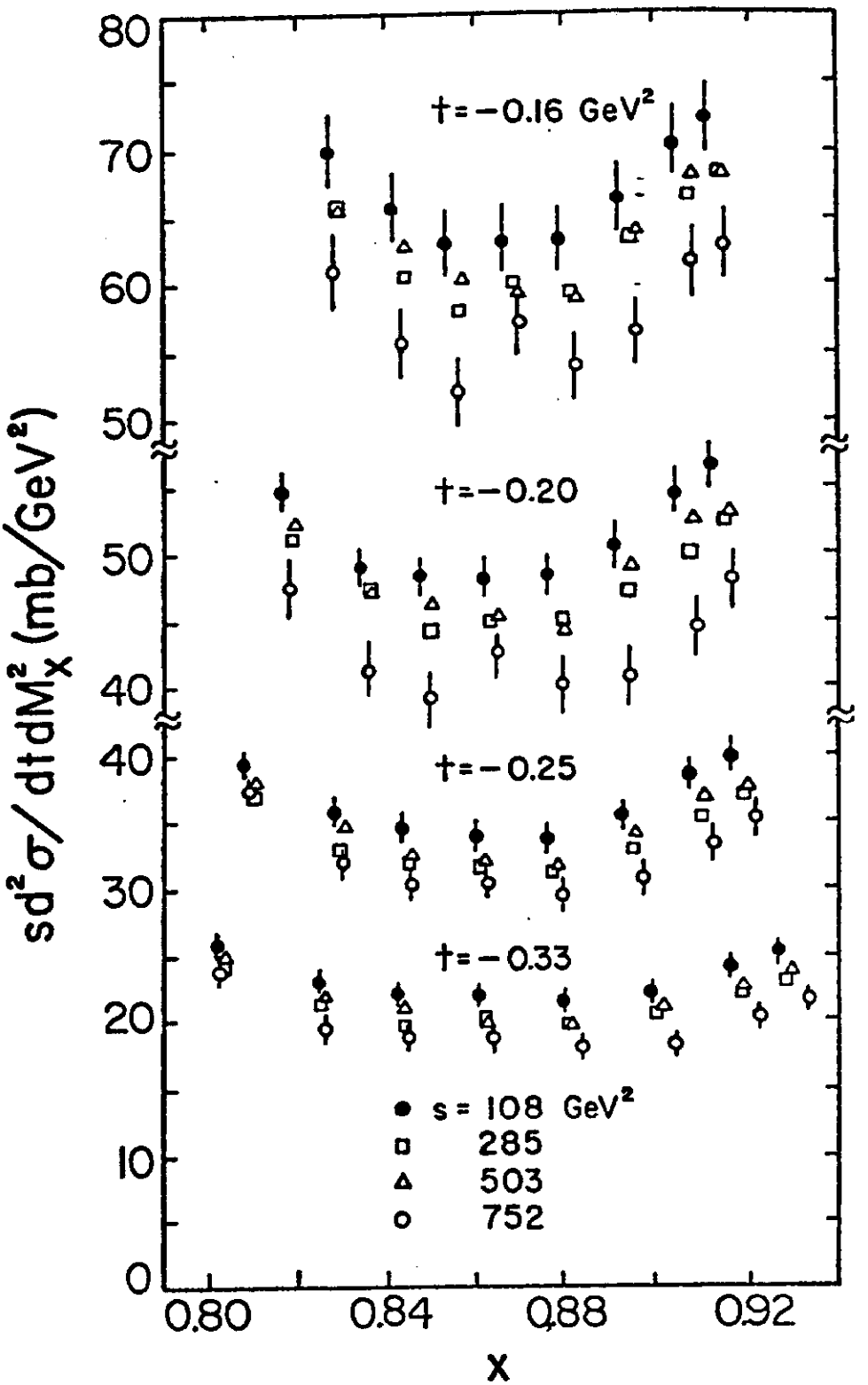
t=−0.16 GeV²
t=−0.20
t=−0.25
t=−0.33
s = 108 GeV²
285
503
752
sd²σ/dtdM²x (mb/GeV²)
X
0.80
0.84
0.88
0.92
0
10
20
30
40
50
60
70
80

FIG. 36

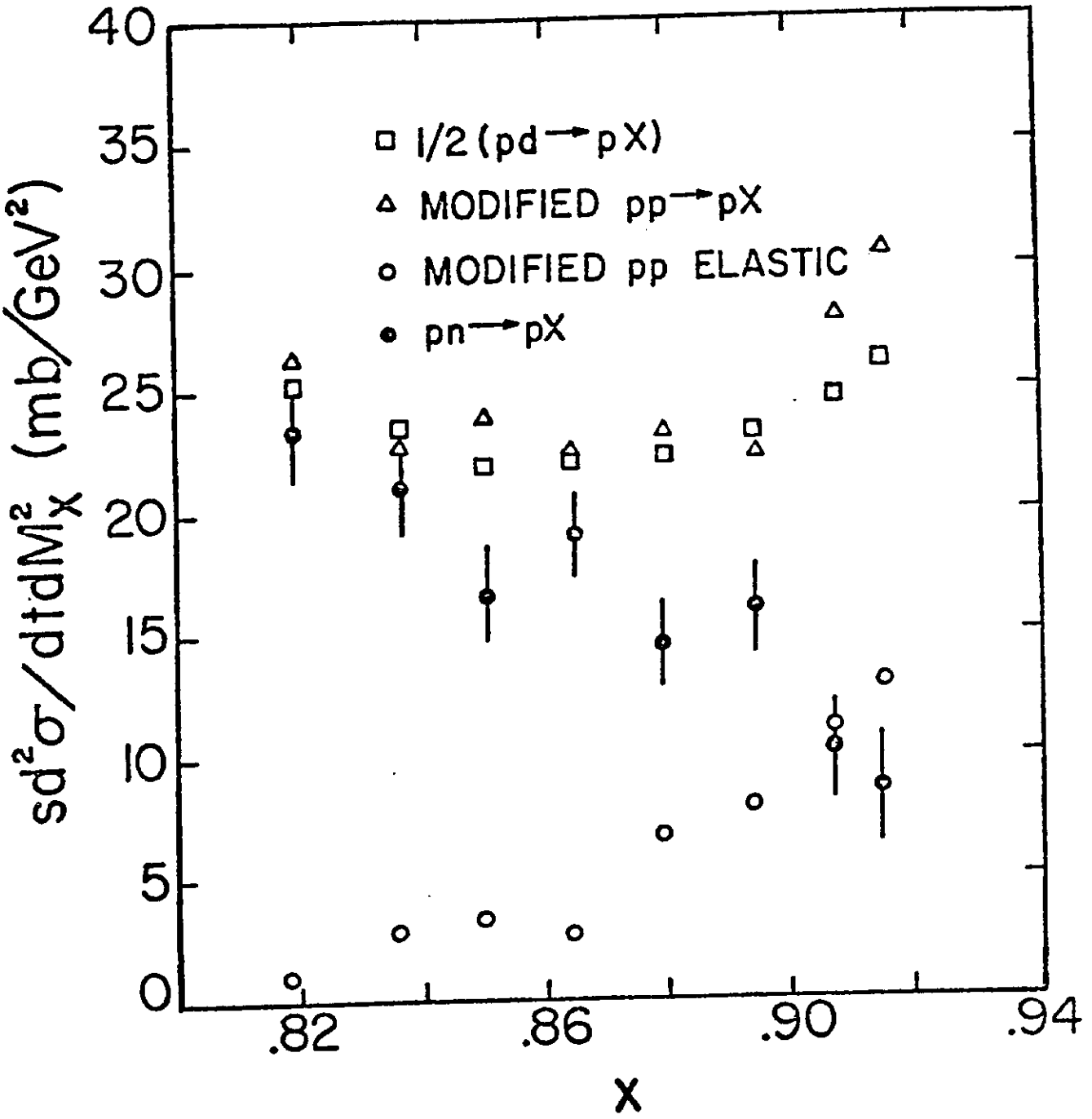
40
35
30
25
20
15
10
5
0
.82
.86
.90
.94
X
$sd^2\sigma/dtdM_X^2$ (mb/GeV^2)
□ 1/2 (pd → pX)
△ MODIFIED pp → pX
○ MODIFIED pp ELASTIC
● pn → pX

FIG. 37

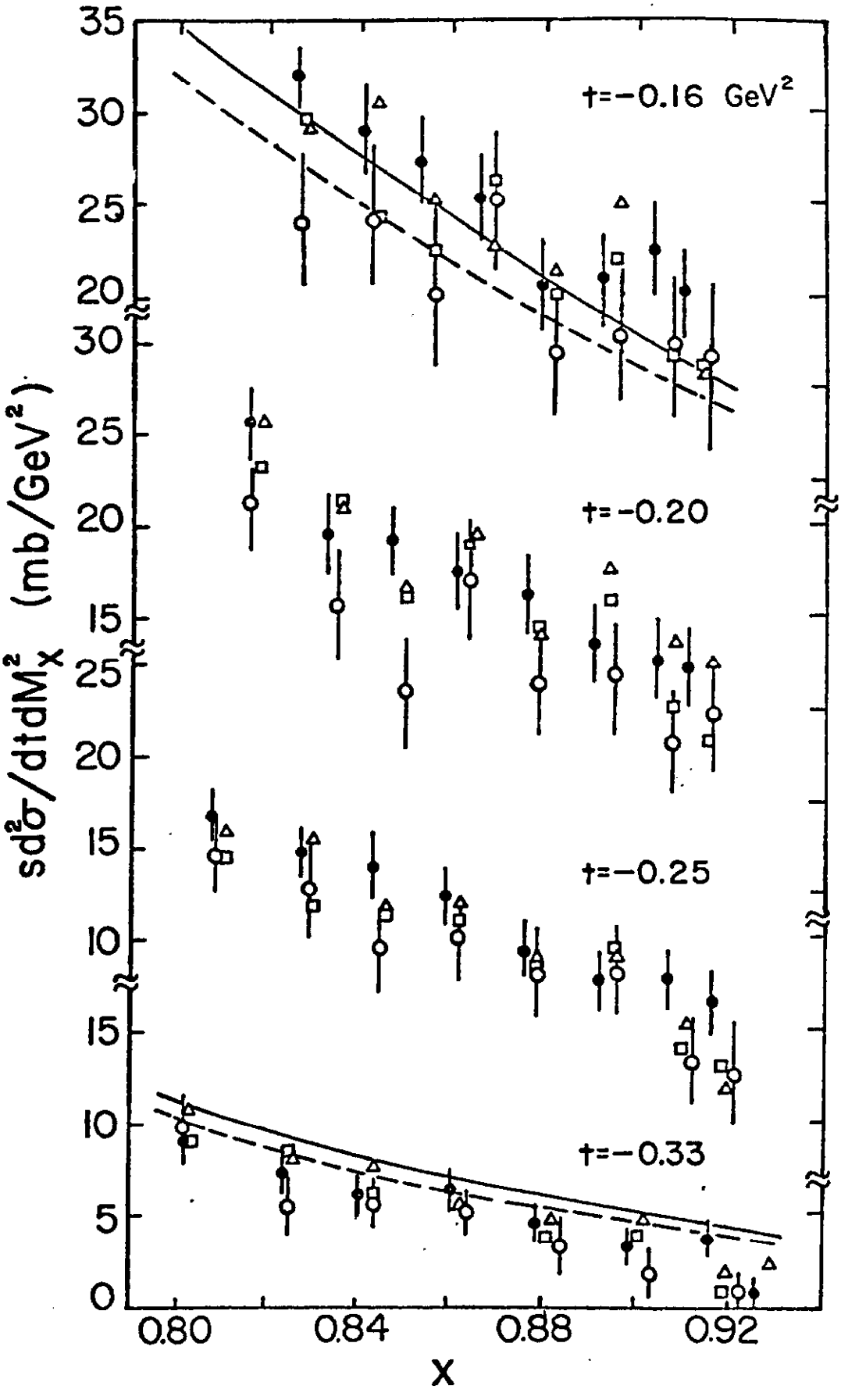
t=−0.16 GeV²
t=−0.20
t=−0.25
t=−0.33
s d²σ/dt dM²x (mb/GeV²)
X
0.80
0.84
0.88
0.92
35
30
25
20
15
10
5
0

FIG. 38

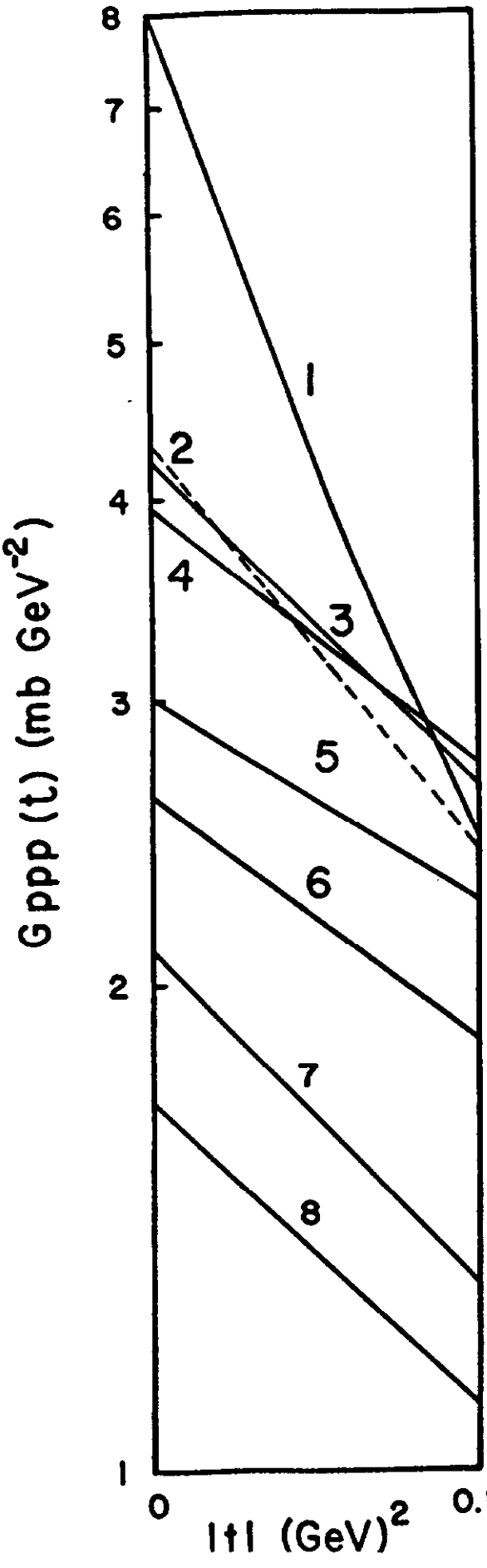

FIG. 39

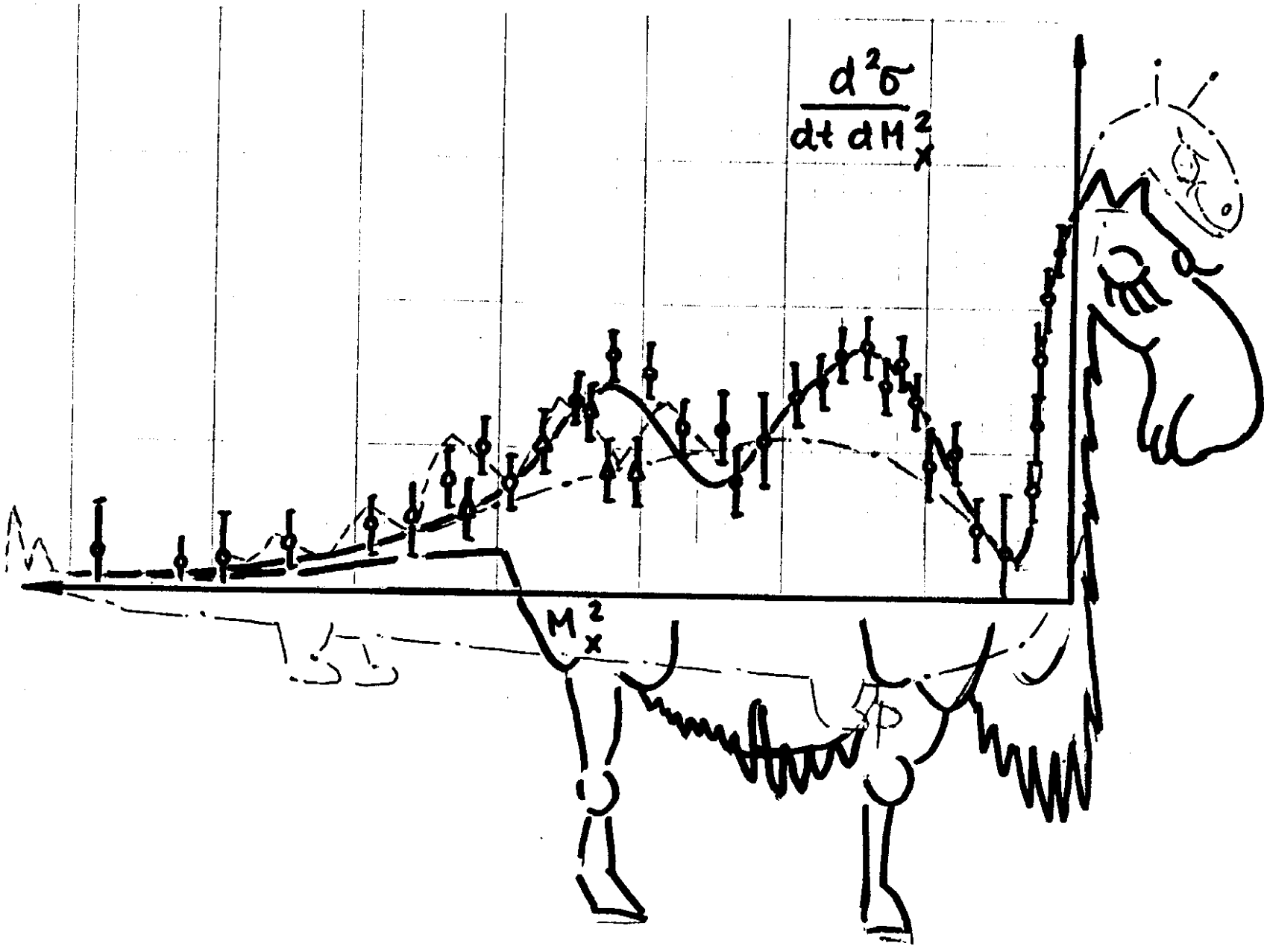

FIG. 40